NAECON '77

Proceedings of the IEEE 1977 National Aerospace and Electronics Conference

GLOBAL POSITIONING SYSTEM USER EQUIPMENT SESSION

The first GPS user session for the NAVSTAR satellite navigation program

ORGANIZER: Steve F. Russell, Collins Avionics Division, Rockwell International

MODERATOR: Maj. Kenneth A. Myers, USAF

NAECON '77

77CH1203-9 NAECON

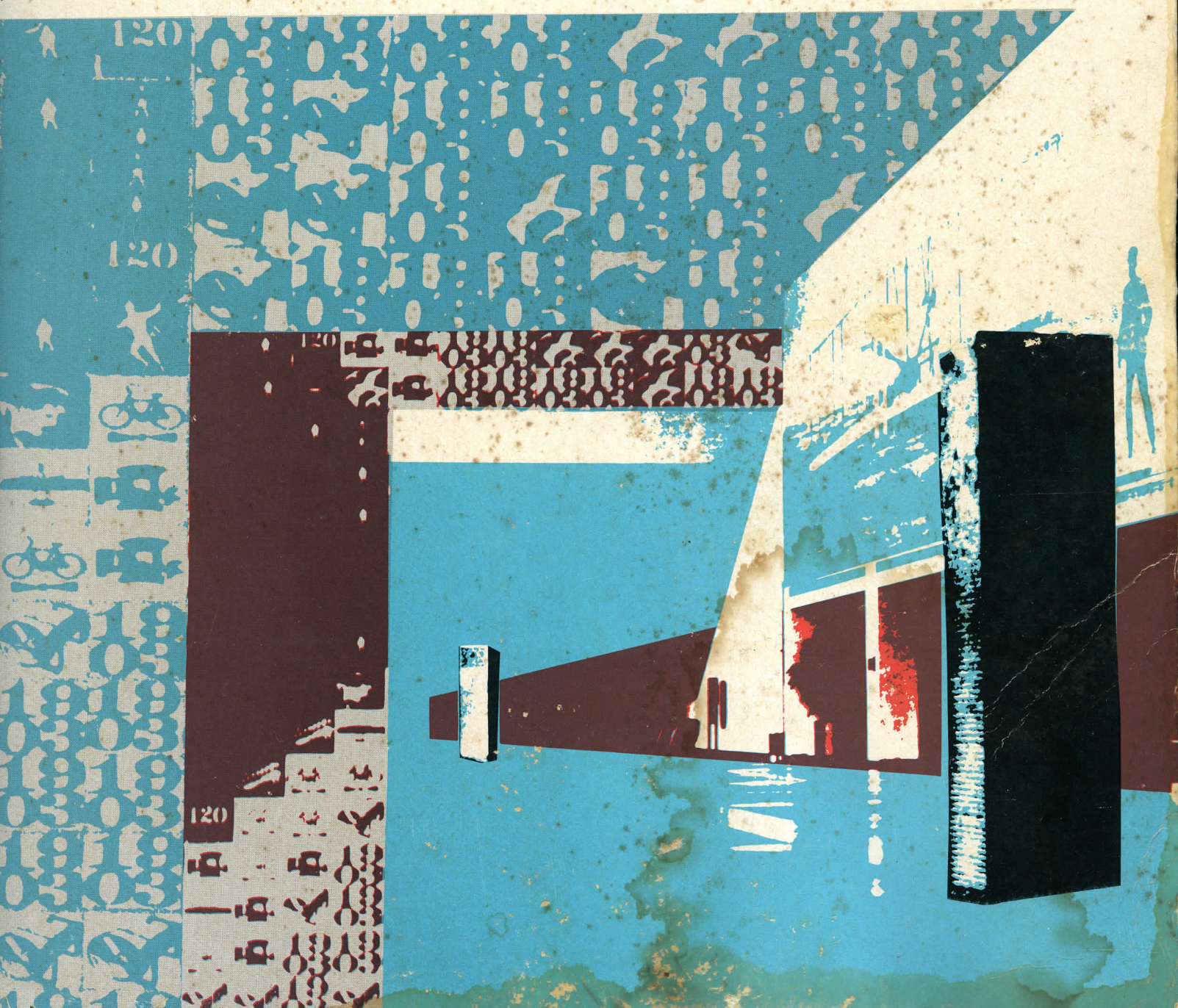

Proceedings of The

IEEE 1977 National Aerospace and Electronics Conference

NAECON '77

Steve F. Russell
Collins Div.
Rockwell Int.
Cedar Rapids, Iowa

Held at the Dayton Convention Center
May 17-19, 1977

Sponsored by

The Institute of Electrical and
Electronics Engineers
Dayton Section
Aerospace and Electronic Systems Society

with participation by

American Institute of Aeronautics
and Astronautics
Armed Forces Communications
and Electronics Assoc.
Association of Old Crows
Institute of Navigation
Scientific Research Society
of America

77 CH1203-9 NAECON

Paper Selection Criteria

NAECON '77 PAPERS COMMITTEE

Chairman	Cheryl L. Zelasco
Assistant	Erwin C. Gangl
Secretary	Sandra L. Clark
Digital Technology	Joseph E. Gebele
Flight Essential Avionics	Paul J. Logus
Engineering Systems	Robert C. Perdzock
Life Cycle Considerations	W. Richard Krupa
Command, Control and Communications	Lt Col Frank L. Cloutier
Commercial Applications	Dr. Chandler A. Phillips
SensorlWeapon Technology	Dr. Robert L. Boggess
Software Engineering	Lt Col Harold C. Falk

NAECON '77 is jointly sponsored by the Dayton Section and the Aerospace and Electronic Systems Society of the IEEE with participation by the Dayton-Cincinnati Section of the American Institute of Aeronautics and Astronautics, Dayton Section of the Institute of Navigation, Kittyhawk Club of the Association of Old Crows, Dayton-Wright Chapter of Armed Forces Communications and Electronics Association, and Sigma XI Dayton Laboratories Branch of the Research Society of America.

The NAECON '77 Record is a publication of the IEEE Aerospace and Electronic Systems Society and is pUblished in conformance with and pursuant to the policies of the society.

The NAECON '77 Record is exempt from the requirement for individual export license under the terms of Title 22, Subchapter M, Article 125, 30-2-2 of the Regulations of the U.S. Department of State, as amended 1 March 1960.

Library of Congress Card Number 61·2171

Published by the Institute of Electrical and Electronic Engineers, Inc., 345 East 47th Street, New York, New York 10017.

The selection of papers for **NAECON** '77 was the work of teams that included, in addition to the Organizers, the sponsoring technical societies' officers, and ASD experts in the subject technical field.

Papers were selected, from abstracts submitted in response to the Call for Papers, on the basis of disclosing new developments that show significant promise of overcoming what were judged to be principle obstacles in the current or future implementation of a technology. A few of the speakers were invited, as outstanding authorities in their fields, to complement the technical program put together from the submitted abstracts.

Unless otherwise indicated, all papers are considered as having been received February 15, 1976.

Cover Design by
Ed Burke
IEEE-AES Transactions
Art & Layout Editor

NAECON Records are available from either
IEEE Service Center,
445 Hoes Lane, Piscattaway, New Jersey 08854
or
IEEE 140 E. Monument Avenue, Dayton, Ohio 45402

Price and availability of NAECON Proceedings for prior years:

(Subject to prior sale)

1955	$15.00 (Digest)
1957	$15.00
1958	15.00
1960	15.00
1961	15.00
1962	15.00
1963	15.00
1964	15.00
1965	15.00
1966	15.00
1967	15.00
1968	15.00
1969	15.00
1970 (70-C-14-AES)	15.00
1971 (71·C-24-AES)	15.00
1972 (72·CH0606-4-AES)	15.00
1973 (73-CH0735-1-AES)	15.00
1974 (74-CH0854-O-NAECON)	16.00
1975 (75-CH0956-3-NAECON)	17.00
1976 (76-CH1 082-7-NAECON)	18.00

Table of Contents

•Abstract only

Authors Index

S

T

TRW 1078

V

W

Y

Z

GLOBAL POSITIONING SYSTEM USER EQUIPMENT

ORGANIZER: Steve F. Russell

AND

MODERATOR: Maj. Kenneth A. Myers

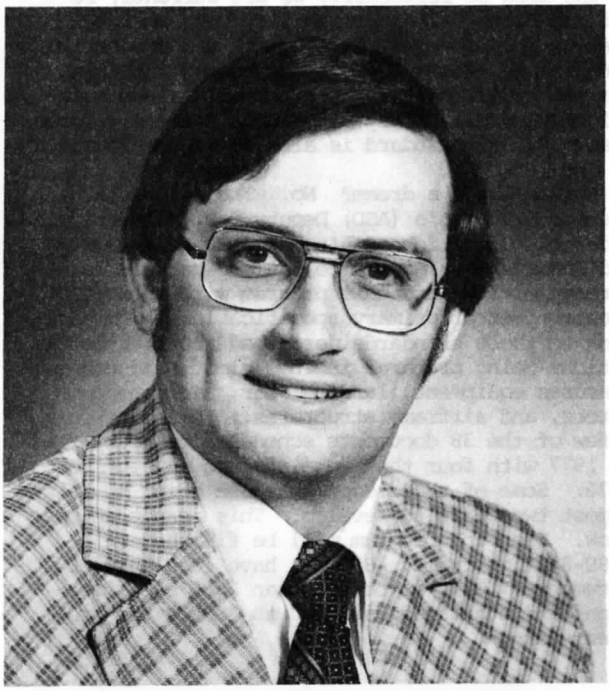

Mr. Steve F. Russell, Collins Avionics Division, Rockwell International.

Mr. Russell received his BSEE from Montana State University in 1966 and an MSEE from Iowa State in 1973 where he is now finishing a Ph.D. dissertation. He is currently with the Collins Avionics Division of Rockwell International as a signal processing analyst on the GDM/GPS program.

Mr. Russell's primary technical interests are in signal processing, spectral analysis, and noise measurement theory. He has six years of experience in RF circuit and system design with emphasis on receivers and low-noise design. Additional experience includes two years as an instructor in Electronic Technology at Iowa State University.

Mr. Russell is a member of IEEE, Eta Kappa Nu, Phi Kappa Phi, and Sigma Xi. He is also the author of a monograph–Noise and Sensitivity-Measurement theory for Receiving Systems and Circuits, in press.

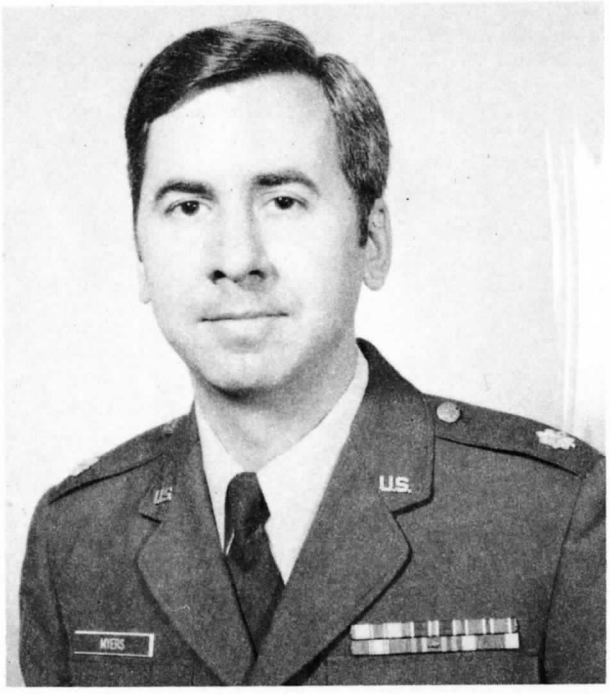

Major Kenneth A. Myers received his B.S. in Aerospace Engineering from The Pennsylvania State University in December, 1964. He entered active duty in June, 1965 at the Air Force Institute of Technology (AFIT), Wright-Patterson AFB, Ohio, where he received an M.S. in Astronautical Engineering in June, 1967. During the next four years he participated in a number of space project activities in the Defense Systems Applications Program at Hq SAMSO, Los Angeles AFS, California. He returned to school in September, 1971, in an AFIT Civilian Institutions Program at the University of Texas at Austin and received in the PhD degree in Aerospace Engineering. He reported to the Aerospace Research Laboratories at Wright-Patterson AFB, Ohio, in December, 1973, serving as a Group Leader in the Applied Mathematics Research Laboratory. In February, 1975, he was transferred to the Air Force Avionics Laboratory, Reconnaissance and Weapon Delivery Division, where he is currently serving as the GPS Technology Program Manager. His research interests include estimation and control theory and satellite navigation.

RADIO/INERTIAL IN FLIGHT CALIBRATION

John A. Graff, Dr. Robert H. Bryant

Boeing Aerospace Company, Seattle, Washington

ABSTRACT

This paper describes the technique of in flight strapped-down inertial alignment and low cost instrument calibration through the use of high iteration rate, high accuracy radio navigation signals such as GPS. The concept of an expendable inertial navigation system in a tactical missile has been made feasible by the combination of low cost microprocessors and the high accuracy radio navigation systems. While the use of update systems to calibrate inertial systems is not a new concept (Boeing used this method in the SRAM alignment filter) the use of low quality, low cost instruments in a strapped-down configuration is relatively new. In the first case the SRAM gyros are relatively high quality rate integrating instruments and are mechanized in a gimballed system. The calibration filter in the case of the lower cost instruments however has to account for errors of much larger magnitude and time variance and for a strapped-down mechanization.

The degree to which these errors can be measured and predicted will be discussed using results from analysis and actual laboratory data--the latter using both rate gyros and low cost rate integrating instruments.

The relative effects of the update characteristics will be discussed. For example, what are the benefits of going thru a filter cycle every five seconds instead of every 20 seconds. What benefit does velocity provide when frequent accurate position updates are available.

Also the benefits of using a high quality strapped-down system which is being updated by a radio navigation system for calibration of a low cost system will be discussed.

HIGH PERFORMANCE ANTENNA ASSEMBLY

Robert J. Prickett

Raytheon Company, Goleta, California 93017

ABSTRACT

The airborne HPAA is able to receive signals from four satellites simultaneously while minimizing the effects of interfering emitters. Four independent, simultaneous beams can be formed anywhere in the hemisphere above the aircraft, positioned by computer commands, or squinted a fraction of a beamwidth away from the satellite to null the signal from a jamming source. The HPAA has demonstrated the ability to provide as much as 25 dB improvement in anti-jam capability when compared to an omnidirectional antenna.

The High Performance Antenna Assembly (HPAA) is a part of the Generalized Development Model (GDM) User Equipment of the Global Positioning System. This User Equipment is designed to operate in an environment such as that shown in Figure 1. The environment typically contains several widely spaced satellites and one or more interfering transmitters.

The HPAA is designed to receive signals from four satellites simultaneously while suppressing interfering noise. The technique employed is to form four independent, simultaneous pencil beams that can be located anywhere in the hemisphere above the user aircraft. These beams can receive both frequencies (1.575 and 1.225 GHz) simultaneously. The narrow beams provide at least 10 dB antijam capability in Mode A when the jammer is not located in the main beam. In this mode the beam is pointed directly at the satellite, and no effort is made to optimize jammer rejection. If instead the HPAA is operated in Mode B, the main beam is then squinted away from the satellite a fraction of a beamwidth to place the jammer in a null in the antenna pattern. In this mode, a 25 dB antijam improvement (compared to an omnidirectional antenna) is possible for many situations.

The physical location of the HPAA on the C141 aircraft is shown in Figure 2. The planar array is attached to the external surface of the aircraft. The RF cable bundle passes through the aircraft skin in a stuffing tube and continues to the electronic housing which contains the remainder of the HPAA equipment. Four RF cables and two control lines run aft from this housing to the remainder of the GDM system located on pallets in the aircraft.

Figure 3 is the top level block diagram of the HPAA. The three major components are the array, beam forming unit (BFU) and beam control unit (BCU). Each of these items will be discussed in some detail. The power conversion unit employs standard dc to dc converters to supply ±5 V and ±12 V from the 28 V input power. This power is used to operate the BFU and BCU as well as the preamplifiers mounted on the electronic housing.

The antenna is a 6 by 6 array of annular slots backed by cavities. Each set of slots is fed by a 90-degree hybrid coupler so that right hand circular polarization is produced. A portion of the array face, showing some of the elements and hybrid couplers, can be seen in Figure 4. Each of the circular slots is resonant over a frequency range of approximately 100 MHz. Use of such a structure provides considerable frequency rejection of unwanted signals, and the resonant circuit also allows the elements to be made smaller. A photo of the complete array with integral aerodynamic fairing is shown in Figure 5. It should be noted that the array face could have been made conformal to largely eliminate the fairing, but a planar array was used for the GDM to reduce design cost.

The BFU, BCU and PCU are mounted in a single housing, and the preamplifiers are placed on the outside of this housing. Figure 6 shows the

completed inboard assembly. All of the microwave hardware is contained in the Beam Forming Unit. (See Figure 7.) The lens module consists of two orthogonal stacks of six lenses each. The lenses, printed on titania ceramic to reduce the size, are of the constant time-delay Rotman type. The Rotman lens has the advantage over many other beam forming networks that its beams do not change direction as frequency is varied. This characteristic makes it possible to receive the two frequencies L1 and L2 simultaneously without degrading performance at either frequency. Inputs from the 36 elements in the array are fed into the lens module. The output of this module is a matrix of 32 primary beams covering an entire hemisphere. Since not all beams are to be used simultaneously the 32 lines are fed into a switch matrix where four four-beam groups are selected for final processing. The switch matrix is made up of interconnected groups of SP5T switches (one arm going to an internal termination) and SP8T switches. PIN diodes are used as switching elements so that switching can be done rapidly enough to compensate for aircraft motion.

If only the 32 primary beam positions were employed, as much as 6 dB in sensitivity would be lost when the satellite was at some intermediate positions. Even more important it would not be possible to squint the beam to improve antijam performance. Therefore, each four-beam cluster is routed into a fine steering module. This module is a four-way variable power combiner. Each of the four paths is independently variable. If these paths are varied in the correct ratios, a grid of intermediate beam positions can be formed within each cluster of four primary beams. In the HPAA, a 16 by 16 grid of intermediate beams can be formed by each fine steering module. This expands the number of possible beam positions from the 6 by 6 grid (with corner beams omitted) of primary beams to a 80 by 80 grid including all of the intermediate positions. The output of each fine steering module in a single sum beam. The resulting four sum beam signals are then amplified and routed to the GDM receivers. Figure 8 shows the individual components (lens stack, switch matrix and fine steering module) that are used in the Beam Forming Unit.

The third major part of the HPAA is the Beam Control Unit (BCU). This unit accepts mode information and four beam position commands, calculates beam positioning commands for the squint function (Mode B), and outputs beam position commands for each beam. The BCU receives two types of commands from the central processor in the GDM. First is a group of four beam positioning commands, and second, for each beam, a mode command, either A or B. If Mode A is commanded, the BCU converts the beam position to specific control signals to the BSU. If Mode B is selected, the BCU calculates repositioning commands to minimize the interference level as determined from voltages received from the preamplifiers (AGC levels).

The BCU block diagram is shown in Figure 9. The heart of the unit is the Central Processing Unit consisting of an Intel 8080 in the SBC 80/10 configuration. Beam position commands, mode commands and timing signals are received over a single bus, converted to the proper format in a 1553 interface circuit and input to the CPU. Four analog AGC signals (one for each beam) are converted to digital words and then sent to the CPU on command from that unit. All of these inputs are processed in accordance with programs stored in the 4K EPROM memory. The CPU then outputs newly formatted beam pointing commands to the switch driver boards through a group of eight output ports. The CPU also transmits a status report, through a FIFO circuit, back to the GDM computer upon receipt of a command from the computer.

The entire HPAA was assembled and tested as a unit on the Raytheon antenna range. For this testing the antenna was mounted on a cylindrical aluminum section simulating that portion of the aircraft near the array. The electronic housing was mounted within the cylinder as would be the case in the final installation. Tests were conducted of five major parameters: beam shape (including beamwidth, sidelobe level and null depth), beam pointing direction, polarization, system gain (excluding preamplifiers), and Mode B nulling performance.

Data for the first three items were taken as a function of frequency to determine performance at both L1 and L2. Typical beam shapes at different pointing angles are shown in Figure 10. Mode B was tested at a single frequency by placing a source in the field of view to simulate a jammer. Antenna patterns were then taken with and without the jammer operating, with all other conditions the same.

This data shows that 10 dB improvement in antijam capability relative to an omnidirectional antenna is available over much of the field of view in Mode A. When Mode B is activated antijam improvement greater than 20 dB is possible for most conditions. Results achieved with the HPAA to date show that its use in the GPS will provide significant system benefits in an operational environment.

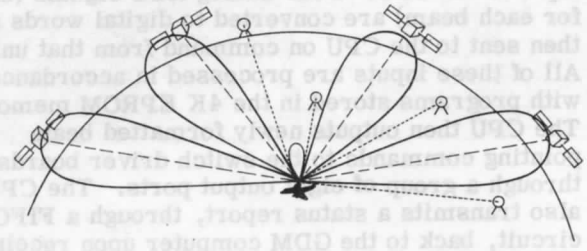

Figure 1. HPAA Environment

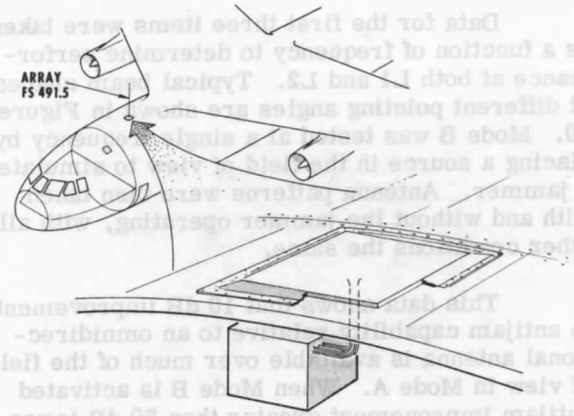

Figure 2. HPAA Location/Installation

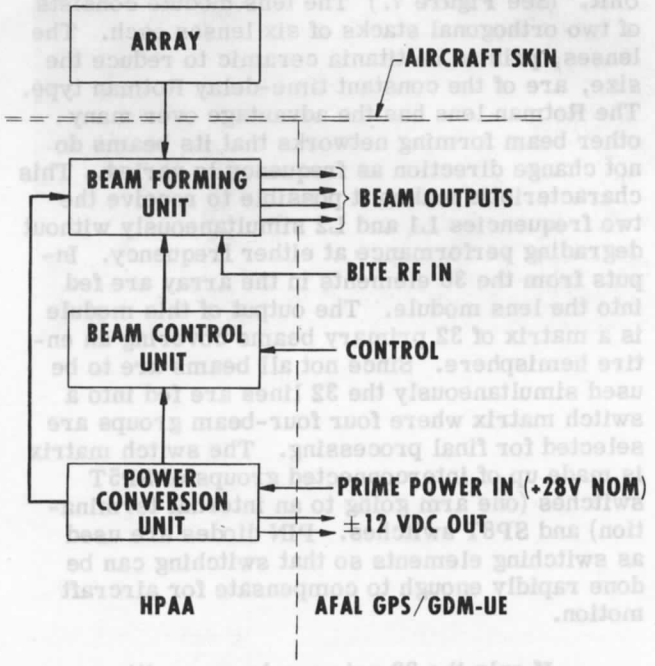

Figure 3. High Performance Antenna Assembly Top Level Block Diagram

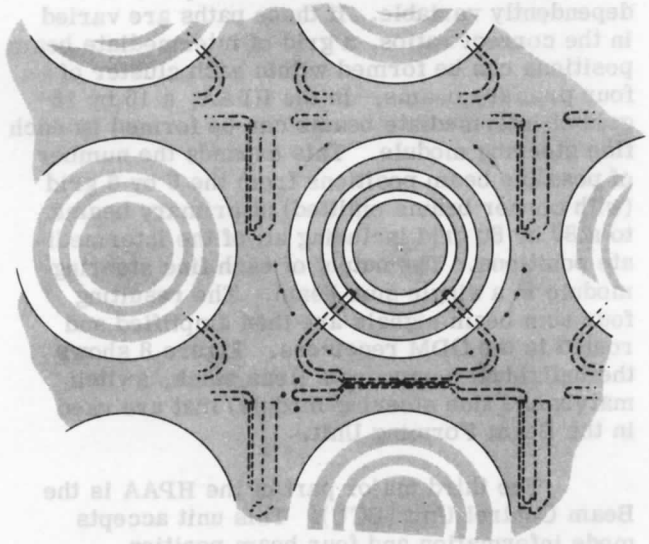

Figure 4. Annular Slots Showing Couplers and Feed Lines

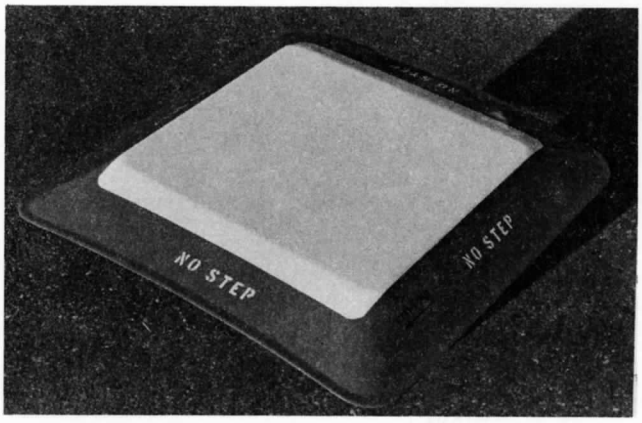

Figure 5. Antenna

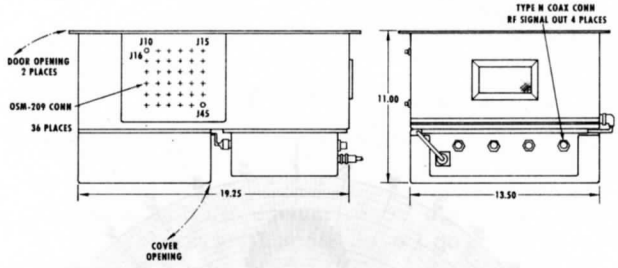

Figure 6. Inboard Electronic Housing

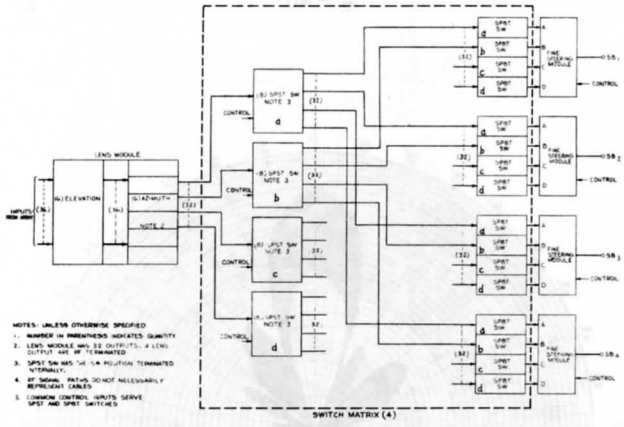

Figure 7. Beam Forming Unit High Performance Antenna Assembly

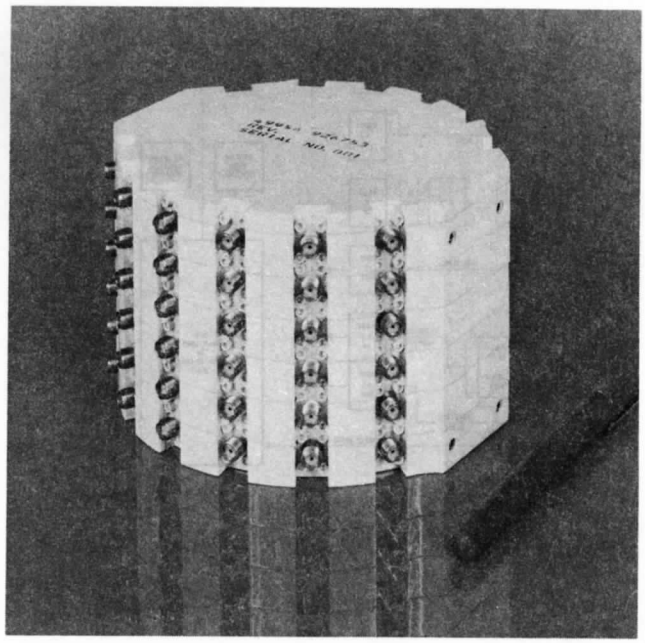

LENS

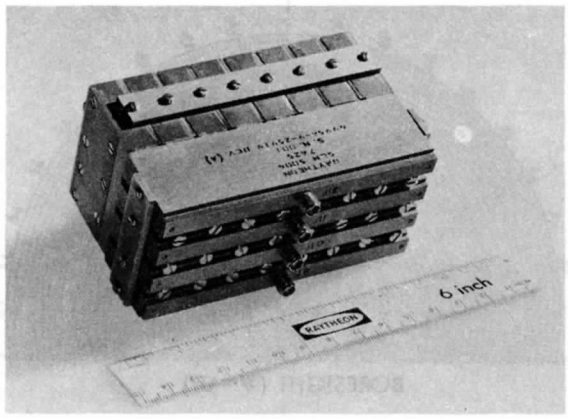

SWITCH MATRIX

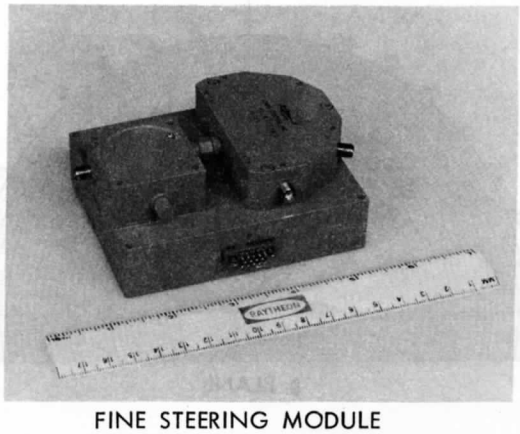

FINE STEERING MODULE

Figure 8. BFU Components

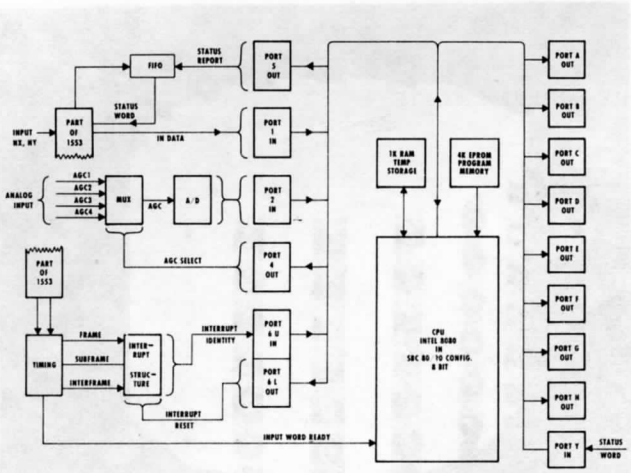

Figure 9. HPAA Controller – Block Diagram

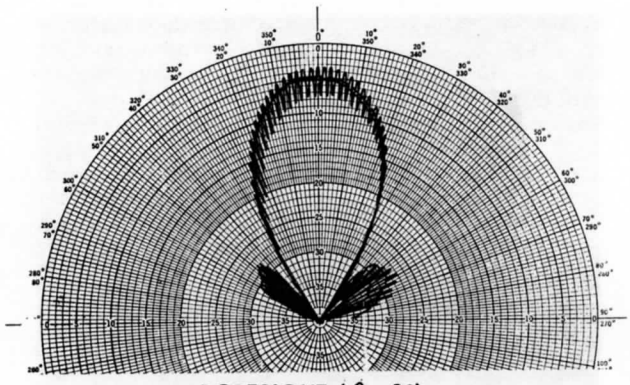

BORESIGHT ($\theta = 0°$)

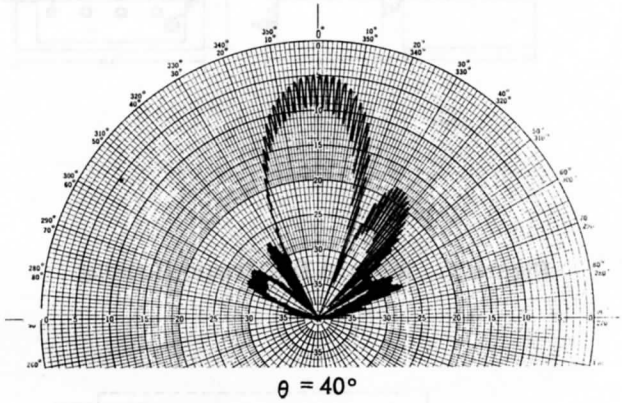

$\theta = 40°$

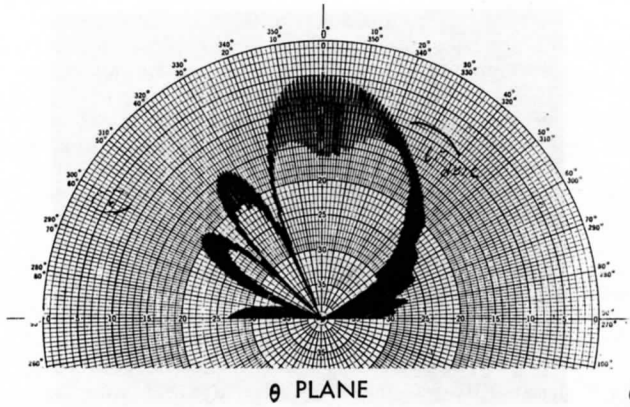

θ PLANE

$\theta = 55°$

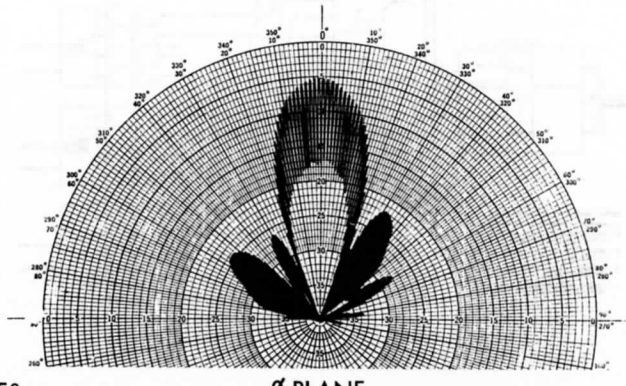

ϕ PLANE

Figure 10. HPAA Beam Shapes at 1.575 GHz

GDM/GPS RECEIVER HARDWARE IMPLEMENTATION

G. L. Bjornsen
W. M. Hutchinson

Collins Avionics Division
Rockwell International

ABSTRACT

This paper describes the receiver hardware implementation for the AFAL GDM/GPS equipment. Included are descriptions of the rf receiver, frequency synthesizer, and signal channel processor. Specific items discussed include receiver bandwidth, wide-band AGC performance, pseudonoise (PN) mixers, code correlation, PN code generator, and digital vco's. Various system issues, as they relate to the GDM/GPS equipment are also addressed.

The GDM/GPS hardware has been partitioned such that it can be configured (under processor control) to represent various GPS equipment configurations for performance evaluation. Also included in this paper is a brief description of an internally generated test signal and its use for system calibration.

INTRODUCTION

GDM/GPS is a versatile test receiver for GPS signals to be used to evaluate potential antijam features in both a laboratory and flight test environment. The antijam features fall into three categories:

1. High performance antenna assembly (HPAA).
2. Inertial aiding of tracking loops to provide narrow loop bandwidths by subtracting out inertially estimated dynamics and tracking the residual difference.
3. Signal processing techniques and tactics such as data aiding, dynamic tracking loop bandwidth adjustment, satellite selection, etc.

These objectives result in a hardware/software design with two major features not common to other GPS user equipments.

1. Four separate rf receivers are provided to receive from each of the four directive beams provided by the HPAA.
2. To the maximum extent possible, the signal processing is provided for in software using a powerful miniprocessor receiver controller with core (reloadable) memory, for all rf and signal processor hardware control; and for all tracking loop, acquisition, and demodulation algorithms. The receiver controller is common to all signal processors, and it thereby offers the capability to interrelate the simultaneous tracking of several satellite vehicles (SV's).

These two features, coupled with the detailed design necessary to allow very narrow tracking loop bandwidths, high J/S signal level environments, and fast recovery to jammer levels, provide the underlying requirements which guided the hardware design presented below.

SYSTEM DESCRIPTION

Figure 1 shows the GPS/GDM system block diagram. The material which follows addresses the receiver subsystem hardware between the HPAA and receiver processor/1553A interface. There are three segments to this equipment:

1. The rf unit which contains four L1/L2 preamplifiers to interface the HPAA, four dual frequency translators to convert the L1 and L2 signals to an if of 71.61 MHz, and an 8 x 5 if switch which provides computer controlled interconnect between any of four SV L1 or L2 signals and any of five signal channel processors (SCP's).
2. The five signal channel processors which convert the if to baseband using pseudonoise (PN) correlators, provide digitally controlled vco's for the carrier and code tracking, provide the code generators, and provide a digital interface to the transfer bus associated with the receiver processor.
3. The receiver processor, which is the minicomputer used to mechanize the tracking loop, acquisition, and demodulation algorithms; to control the receiver subsystem hardware, and to provide time and ephemeris data, pseudorange, and pseudorange rate to the navigation subsystem via the 1553A bus.

Both the HPAA and portions of the navigation processing are covered in accompanying papers. These equipments, therefore, will not be further addressed.

RF SUBSYSTEM

The rf subsystem provides the interface between the HPAA and the five signal channel processors. There are four separate rf channels which convert both the L_1 and L_2 signals to 71.61-MHz if signals and a computer controlled 8 x 5 if switch which allows any of four satellite vehicle L_1 or L_2 signals to be connected to any one or any combination of SCP's. Also contained in the rf unit is the frequency synthesizer which provides all of the reference signals and the master timing signal for the GDM system. The BIT module, when commanded by the receiver processor, outputs simulated satellite signals at the L_1 and L_2 frequencies for injection into the front end of the receiver (at the HPAA) which are used to calibrate the differential delays through the various rf signal channels. In the following discussion and block diagrams, F_0 is defined to be 5.115 MHz.

One rf preamplifier is provided for each of the four antenna beam outputs from the HPAA. The antenna is located away from the GDM system, thus necessitating an rf preamplifier to maintain a low system noise figure. Preselector filters for L_1 and L_2 are provided at the input of the preamplifier to give the desired signal rejection to out-of-band signals. These filters are four pole,

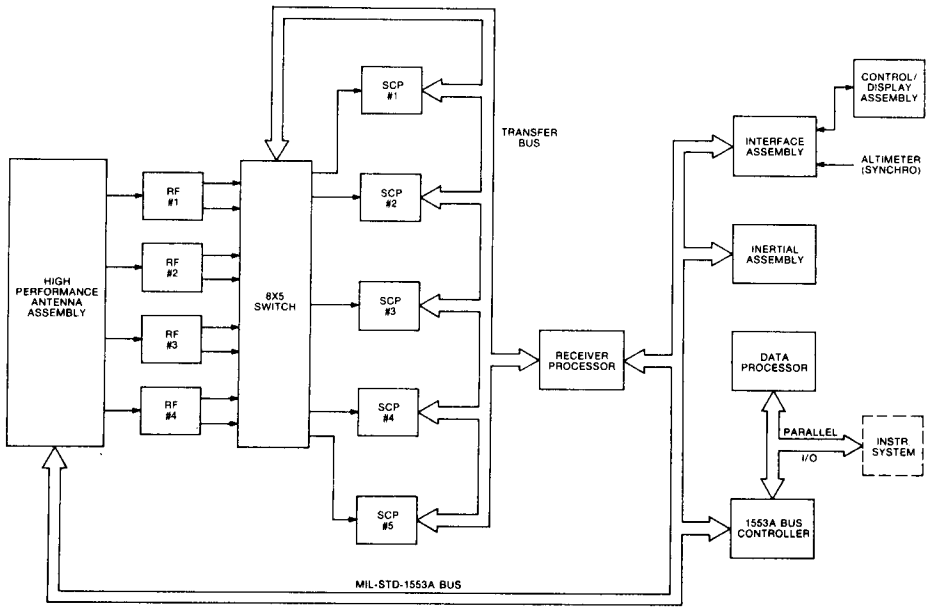

Figure 1. System Block Diagram.

loop coupled coaxial cavity resonator type filters with a frequency response as shown in figure 2. An rf limiter precedes the rf amplifier to prevent overloading and noise figure degradation in the presence of high power pulse jammers. The rf amplifier uses a low noise figure transistor and microstrip construction to provide the required gain and set an overall system noise figure of 3.5 dB. A diplexer at the output of the preamplifier strips off the wide-band AGC voltage, provided by the signal channel processor and diplexed on the rf coax, for use by the HPAA in the squint mode of operation.

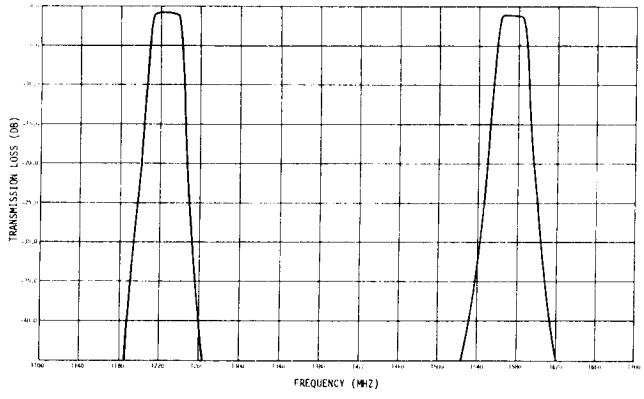

Figure 2. RF Preamplifier Filter Response.

The L_1/L_2 signal from the preamplifier is amplified by low noise rf amplifiers at the input of the rf module. This signal then passes through two ceramic filters, one for L_1 and one for L_2. The frequency response of the L_1 signal filter is shown in figure 3. The L_1 signal ($308F_O$) is mixed with the L_O signal ($294F_O$) to give a 14 F_O if signal which is then filtered and buffered. L2 ($240F_O$) is mixed with the other injection frequency from the synthesizer ($226F_O$) to give the 14 F_O if signal for L_2. The output amplifier drives the 8 x 5 if switch. This amplifier is designed with a low output impedance so

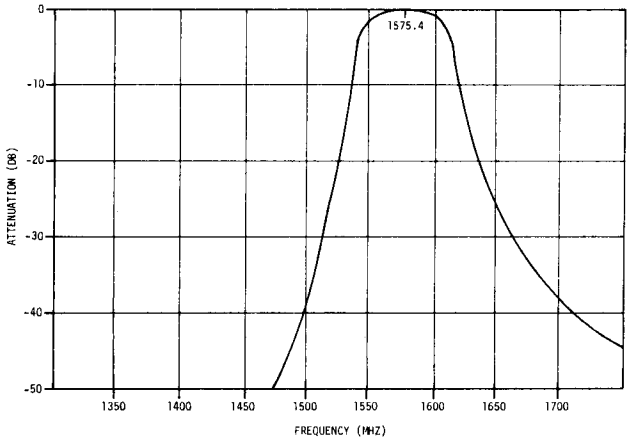

Figure 3. L_1 Signal Filter.

that under processor control if it is desired to connect more than one SCP to a particular rf channel, the signal level does not change appreciably.

The frequency synthesizer contained in the rf unit generates all of the reference signals for the GDM system. A 10.0-MHz oven standard crystal oscillator, made by HP, is the reference standard used by the synthesizer. The synthesizer was designed to be operated with either an internal or external standard. An external 5.0 MHz, or a 5.115 MHz standard with a minor strapping system, can be used as the reference for all the frequencies generated in the synthesizer. Two outputs, $294F_O$ and $226F_O$, are provided as L_O injection and are also used in conjunction with a low-level $2F_O$ output for the generation of the BIT signal. Three high level outputs, $11.5F_O$, $2F_O$-$F_O/80$, and $2F_O$, serve as reference signals for the five SCP's. The 5-ms interrupt, $F_O/25600$, is generated by the synthesizer and is used by the GDM system as the master timing signal.

The BIT module, as shown in figure 4, generates the L_1/L_2, PN modulated rf signal used for calibration of the GDM system. When this module is turned on by the receiver processor, a $2F_O$ reference signal from the frequency synthesizer is applied to a times 7 multiplier which generates a $14F_O$ carrier signal. This carrier is then modulated by a PN code generated in the particular SCP selected by the receiver processor. This PN modulated carrier is then translated to the L_1 and L_2 frequencies with the $294F_O$ and $226F_O$ frequencies from the synthesizer. These two signals are combined to form the composite L_1/L_2 simulated satellite signal.

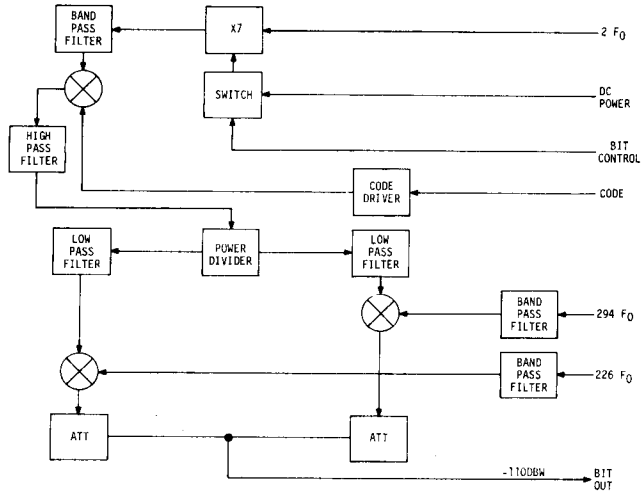

Figure 4. BIT Module.

SIGNAL CHANNEL PROCESSOR

The signal channel processor serves as the analog-to-digital interface between the rf receiver and the receiver processor. The SCP demodulates the received PN code, provides digitized I and Q values to the receiver processor, accepts control information from the receiver processor for code generator and code and carrier vco control, provides built-in-test PN code for system calibration, and provides the wide-band AGC voltage to the HPAA. Five SCP's are used in the GDM system. Four SCP's, during parallel operation, are normally dedicated to the four rf channels with the fifth SCP available for other tasks such as calibration and ionospheric delay correction measurements.

The wide-band if has a bandwidth of 25 MHz (on the same order as the rf receiver bandwidth) to allow passage of the spread spectrum satellite signal with a minimum of band limiting to keep the correlation losses in the PN mixers to a minimum. The AGC loop in the wide-band if maintains a constant output power level, thus controlling the levels into the PN mixers and noise level into the crystal filters. There are two special requirements for the AGC loop. One, the response time of the loop must be relatively fast to prevent blocking or degradation of performance due to high pulse power jammers. Second, when the jammer power level exceeds the thermal noise level and the gain is turned down to maintain a constant output level, the phase shift of the carrier signal must be held to a minimum (less than 5 degrees over a 40-dB range) to prevent the carrier-tracking loop from losing lock as the gain of the receiver is controlled by the jammer. At this point in the receiver system the satellite signal is always below the thermal noise level (on the order of 20 to 30 dB), thus the wide-band AGC operates only on interfering signals and the HPAA can use this voltage to minimize the interfering signal level.

The signal channel processor was implemented with dual correlator channels (figure 5). This allows, except in a high interfering signal level environment, the code- and carrier-tracking loops to operate on independent channels. Channel A is used for the carrier-tracking loop and channel B is used for the code-tracking loop in the coherent track mode. Channel B is used to maintain the correct local PN code position. This is done by offsetting the code by 1/2 chip, alternating the code position 1/2 chip early or 1/2 chip late and maintaining equal power in channel B for both code positions. In the non-coherent track mode, both A and B channels are used to track the incoming signal, one channel early, the other late.

After being amplified by the wide-band if, the signal is correlated in the PN mixers if the local PN code is aligned with the received signal. Two mixers are used in series to recover the carrier of the satellite signal.

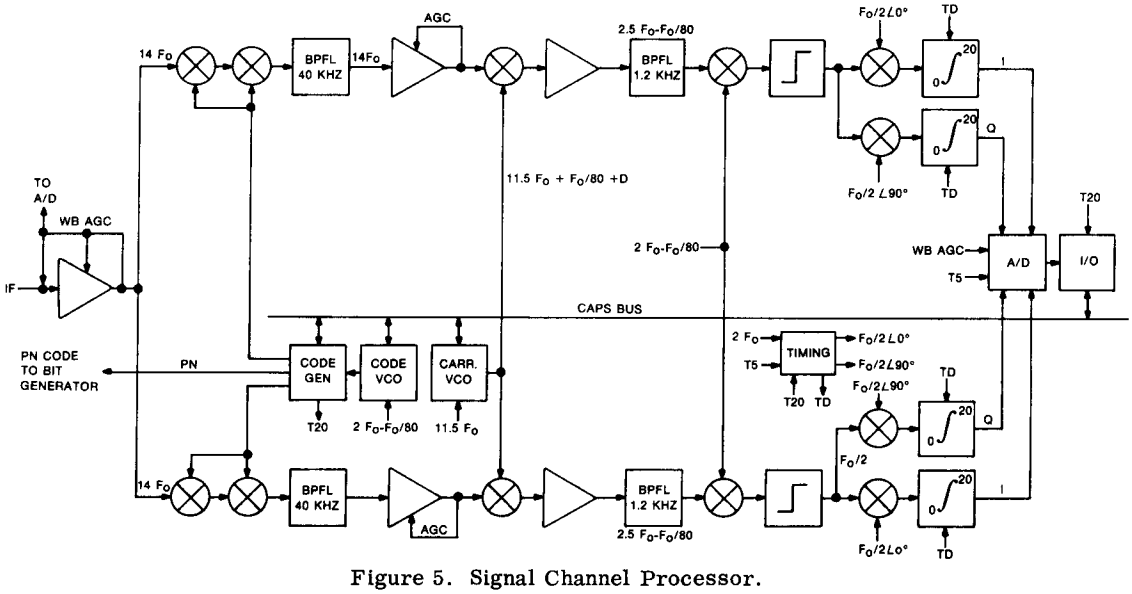

Figure 5. Signal Channel Processor.

The BIT module, as shown in figure 4, generates the L_1/L_2, PN modulated rf signal used for calibration of the GDM system. When this module is turned on by the receiver processor, a $2F_0$ reference signal from the frequency synthesizer is applied to a times 7 multiplier which generates a $14F_0$ carrier signal. This carrier is then modulated by a PN code generated in the particular SCP selected by the receiver processor. This PN modulated carrier is then translated to the L_1 and L_2 frequencies with the $294F_0$ and $226F_0$ frequencies from the synthesizer. These two signals are combined to form the composite L_1/L_2 simulated satellite signal.

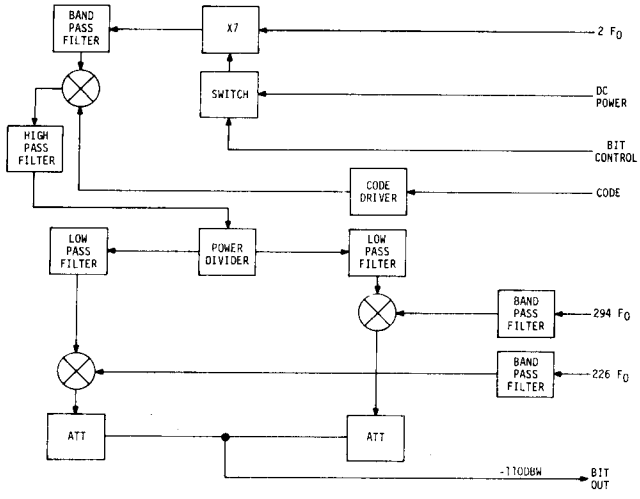

Figure 4. BIT Module.

SIGNAL CHANNEL PROCESSOR

The signal channel processor serves as the analog-to-digital interface between the rf receiver and the receiver processor. The SCP demodulates the received PN code, provides digitized I and Q values to the receiver processor, accepts control information from the receiver processor for code generator and code and carrier vco control, provides built-in-test PN code for system calibration, and provides the wide-band AGC voltage to the HPAA. Five SCP's are used in the GDM system. Four SCP's, during parallel operation, are normally dedicated to the four rf channels with the fifth SCP available for other tasks such as calibration and ionospheric delay correction measurements.

The wide-band if has a bandwidth of 25 MHz (on the same order as the rf receiver bandwidth) to allow passage of the spread spectrum satellite signal with a minimum of band limiting to keep the correlation losses in the PN mixers to a minimum. The AGC loop in the wide-band if maintains a constant output power level, thus controlling the levels into the PN mixers and noise level into the crystal filters. There are two special requirements for the AGC loop. One, the response time of the loop must be relatively fast to prevent blocking or degradation of performance due to high pulse power jammers. Second, when the jammer power level exceeds the thermal noise level and the gain is turned down to maintain a constant output level, the phase shift of the carrier signal must be held to a minimum (less than 5 degrees over a 40-dB range) to prevent the carrier-tracking loop from losing lock as the gain of the receiver is controlled by the jammer. At this point in the receiver system the satellite signal is always below the thermal noise level (on the order of 20 to 30 dB), thus the wide-band AGC operates only on interfering signals and the HPAA can use this voltage to minimize the interfering signal level.

The signal channel processor was implemented with dual correlator channels (figure 5). This allows, except in a high interfering signal level environment, the code- and carrier-tracking loops to operate on independent channels. Channel A is used for the carrier-tracking loop and channel B is used for the code-tracking loop in the coherent track mode. Channel B is used to maintain the correct local PN code position. This is done by offsetting the code by 1/2 chip, alternating the code position 1/2 chip early or 1/2 chip late and maintaining equal power in channel B for both code positions. In the non-coherent track mode, both A and B channels are used to track the incoming signal, one channel early, the other late.

After being amplified by the wide-band if, the signal is correlated in the PN mixers if the local PN code is aligned with the received signal. Two mixers are used in series to recover the carrier of the satellite signal.

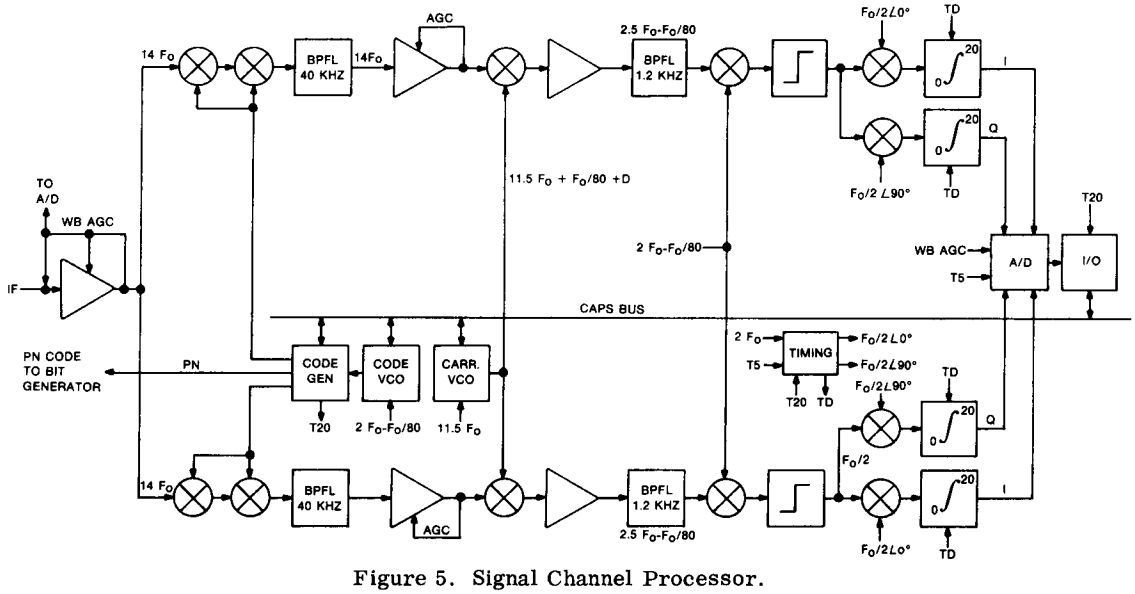

Figure 5. Signal Channel Processor.

This requires some special circuitry in the code generator to drive the two mixers and recover the signal (figure 6); however, this gives 75- to 80-dB carrier suppression to CW interfering signals, assumming 35 to 40 dB of balance in each mixer. The input to the second mixer (C as shown in figure 6) can be any type of signal that will spread the CW component leaking through the first mixer. It is possible for C to be a PN code, or even a frequency such that the mixer products fall outside the subsequent narrow-band filters.

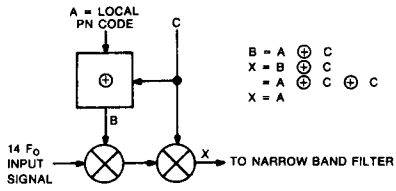

Figure 6. Pseudonoise Mixers.

After the signal is correlated in the PN mixers, it passes through a 40-kHz bandpass crystal filter. At this point in the SCP, the doppler shift of the carrier frequency is removed. The injection frequency is generated by the carrier vco, whose frequency is controlled by the receiver processor. This frequency (11.5 F_O + $F_O/80$ + D, where D represents the doppler shift) is mixed with the if signal to give a second if frequency of 2.5 F_O-$F_O/80$. This signal is further amplified and filtered by a 1.2-kHz bandpass crystal filter. This signal is then mixed with 2 F_O - $F_O/80$, from the frequency synthesizer, which results in a final if frequency of $F_O/2$. These outputs, from the two correlator channels, are fed to the two detector modules which contain the limiters, phase detectors, and integrate-and-dump circuitry.

The limiter is implemented with a zero crossing detector. The phase detectors are implemented with digital exclusive-OR gates. The outputs of the phase detectors are square waves whose duty cycles are proportional to the phase difference between the limiter output and the two reference signals, $F_O/2 \angle 0°$ and $F_O/2 \angle 90°$. The in-phase (I) and quadrative-phase (Q) signals are applied to the integrate-and-dump circuitry. The integration time is controlled by the local code generator so that the integration period (20 ms) coincides with the data bit modulation interval on the received signal. At the end of the integration period, this value is digitized by the a-to-d converter and stored in a RAM for use by the receiver processor. At every T5 interrupt, the running values of the integrators are digitized and stored. This provides a predetection bandwidth of 200 Hz versus 50 Hz when only the dump values are used.

The a-to-d converter uses a high-speed, 8-bit a-to-d converter and at every 5-ms interrupt digitizes all the I and Q values and the wide-band AGC voltage and stores them in the RAM. The receiver processor can access this RAM and retrieve any of the values it needs to perform its required operations.

The heart of the signal channel processor is the code generator and digital vco's which control the code position and carrier frequency. First let us look at the code generator and then the two vco's. The detailed operation of the code generator is too complex to present in this paper, but the features are important and will be discussed.

The pseudorandom sequence of the P code generated in the satellite, is restarted at the beginning of each week and since its cycle is longer than 7 days, it never repeats during the week. The GDM equipment can be turned on and/or restarted at any time during the week. This requires that the local code generator have the capability to reach, or slew to, the correct time of the week very quickly. To do this, three slew commands are provided in the code generator. First is the 3-second slew. This command, controlled by the receiver processor, will cause the code generator to advance in time an amount equal to 3 x N seconds. The maximum value for N is 32768, which equates to 1.1 days. The maximum time required to execute this command is less than a quarter of a second. The second slew command is the 2-ms delay/advance control. Upon receiving this command, the code is set back 40 ms and then advanced 2 x Nms, where N is the value of the command with a maximum permissible value of 511. This command generates a range of control from 40-ms delay to 982-ms advance and is executed in less than 1.2 ms. The third slew command is the fine delay control. Upon receipt of this word, the code generator stops for N cycles (equivalent to N chips of P code), where N is the value in the data word and has a maximum value of 32767. By the use of these three slewing commands, the code generator can be positioned to any time of the week very quickly. The 2-ms delay/advance and 3-second slew commands are multiples of the C/A code (1ms) and thus can be executed without losing lock on the C/A code once it has been acquired.

Six other control features provide the flexibility needed for a GPS test bed such as GDM.

1. Reset Command. Upon receiving this command the code generator starts at the beginning of the week state at the next 5-ms interrupt. In order to assure that no ambiguity exists as to the first cycle after the interrupt, the vco (which supplies the clock signal for the code generator) will be reset and then controlled in phase at the time of the 5-ms interrupt.
2. Satellite Selection. Any one of the presently defined satellite PN codes may be selected.
3. Code Selection. Either C/A or P code may be selected to be used for demodulation of the incoming satellite signal.
4. Early/Late Selection. This allows selection of the code position for the two correlator channels (A and B). In the coherent track mode, channel B is positioned early and late, ±1/2 chip, to determine the correct code position. In the noncoherent track mode, channels A and B are both offset by 1/2 chip, one early and one late.
5. Modulation Control. The capability is provided to select the code output, either normal output or inverted output. The change of state occurs at data bit transition times. This permits the code generator to generate a code with data modulation for test purposes. It also allows for data injection, to be implemented at a later time, for increased GPS performance.
6. End of Week. This is not a commanded feature but takes place automatically. When the end of week occurs, the code generator resets itself to the beginning of the week state and continues with the correct sequence.

There are two vco's in the signal channel processor, the code vco shown in figure 7 and the carrier vco shown in figure 8. The operation of these vco's is straight forward. The receiver processor controls the frequency of the digital vco through the data bus. This frequency is then mixed with a frequency from the GDM frequency

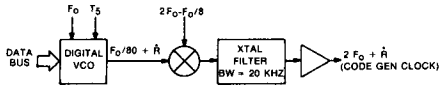

Figure 7. Code VCO.

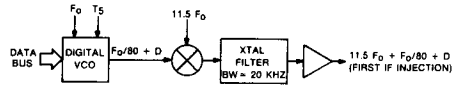

Figure 8. Carrier VCO.

synthesizer, passed through a crystal bandpass filter which passes the correct frequency and filters out all the undesired mixer products, and is buffered and applied to the code generator or provided as the injection frequency to the if modules. The $\dot{R}$ in the code vco block diagram represents the code velocity or doppler shift on the 10.23 MHz ($2F_O$) P code chipping rate. The D term in the carrier vco represents the doppler shift on the carrier frequency for L_1 or L_2 depending on which frequency is being tracked.

The digital vco is identical for both the code and carrier vco. A block diagram is shown in figure 9. The received digital data from the receiver processor is loaded into the B register. During the following sample interrupt time it is modified and loaded into the BA register. The same data is utilized to load into the BA register till new data is received from the receiver processor. The digital vco has a frequency range from 0 to 256 kHz. The required nominal output frequency of the digital vco is $F_O/80$ (≈64 kHz) and the data from the receiver processor is the deviation from this nominal frequency. This means that the data must be modified (in hardware) before being loaded into the BA register so that a zero frequency command results in an output frequency of $F_O/80$.

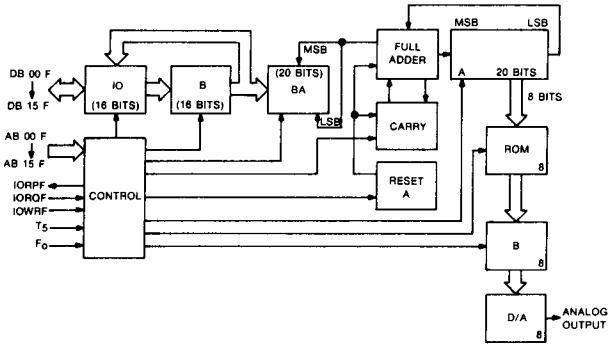

Figure 9. Signal Channel Processor Digital VCO.

Let us look at how the output frequency is generated. Assume the data in the BA register is N. The serial addition is performed at a rate equal to $F_S = F_O/20$, where F_O is equal to 5.115 MHz and the result module, 2^{20}, is kept in the A register. The expression is $A = A + BA$. Every sample time ($F_S = F_O/20$), the most significant eight bits of the A register are translated through ROM (sine table) and d/a converts during that sample time interval. Over sample interrupt periods, the outputs of d/a converter appear as an analog signal with frequency F. The relationships between N (in the BA register) and the output frequency F of the d/a converter are defined as:

$$F = \frac{NF_S}{20} \tag{1}$$

$$= \frac{NF_O}{2^{20} \cdot 20} \text{ Hz} \tag{2}$$

$$\text{or} \quad N = 20 \cdot 2^{20} \cdot \frac{F}{F_O} \tag{3}$$

With sample interrupt frequency $F_O/25600$, equation (2) can also be expressed by cycles/interrupt, it is

$$F = \frac{N \cdot 1280}{2^{20}} \text{ cycles/interrupt} \tag{4}$$

The smallest frequency change occurs when delta N = 1 and substituting N = 1 in equation (2) yields 0.244 Hz. Only 16 bits are available on the transfer bus for data and having a requirement to generate ±10-kHz frequency shift from nominal for the carrier vco, the 16 bits were positioned such that the LSB was equal to 2. This yields a frequency range of ±16 kHz with a frequency resolution of approximately 0.5 Hz. If we now look at this control in terms of cycles/interrupt, substituting N = 2 in equation (4) yields F = 0.00244 cycles/interrupt. Realizing that the vco frequency can be changed every interrupt, how does this relate to the code clock frequency or more important code position control? The code generator clock is $2F_O + \dot{R}$. Each P chip, or code clock cycle, is approximately 97.75 ns ($\frac{1}{2F_O}$). Using the lowest frequency, in terms of cycles/interrupt, it is possible to change the code position with a resolution of a quarter of a nanosecond (97.75 ns/cycle x 0.00244 cycles/interrupt = 0.244ns).

This phase change of the code clock, and ultimately the code position change, is translated directly to the code generator. This comes about because the digital vco output frequency ($F_O/80 + \Delta F$) and phase is translated up to the desired frequency and no multiplication of frequency or phase noise takes place. This method of translating up the lower digital vco frequencies to the desired frequencies, provides signal frequencies with essentially no phase noise. This is very important to the performance of the code and carrier-tracking loops implemented in the receiver processor.

RECEIVER PROCESSOR

The receiver processor services the five SCP's. It accepts a/d converted I and Q samples from each channel every 5 ms. The I and Q values are processed as $I^2 + Q^2$ for square law detection and as I x Q for Costas loop carrier-tracking detection. Following software filtering, the detected signal is interpreted as hardware vco commands to the SCP digital vco's, or as acquisition pass/fail data with corresponding code generator indexing commands. The receiver processor also provides GPS pseudorange data to and accepts system control from the 1553A bus which is under the control of the nav data processor. The 50 b/s data demodulation, blocking, parity checking, and Z-count interpretation is also provided in the receiver processor software. The receiver processor is a Collins CAPS-4 flight computer, whose operational characteristics are summarized in table 1.

Figure 10 shows an overall block diagram of the receiver processor. The bridging function between the 1553A bus, which services the nav subsystem, and the

Table 1. CAPS-4 Summary Characteristics.

Word length	
Data	16 and 32 bit variables
Instructions	8-bit (short) 16, 24, 32, 40 bit (long)
Number of instructions	96 standard, unlimited user defined
Addressability	64K words (16 bits per word)
Memory access	Direct
Data area descriptions	16 local variables (LENV) used for storage and indexing 256 extended local variables 16 base values in main memory 64K global variable addressing Accumulator stacking
Stacking operations	Accumulator stacking Local variable stacking (dynamic allocation) interrupt stacking
Typical execution times	Add (single/double) 1.2/3.0 μs Multiply (single/double) 6.1/16.7 μs Divide (single/double) 6.9/30.5 μs
CPU power dissipation	25 watts typical

Table 2. Normal Mode Sequence.

Code generator initialization
Calibration
C/A code acquisition
Carrier-track initialization
Data bit synchronization
Code-track initialization
Data frame synchronization
Time-of-week determination
Code generator slew
P-code track (carrier and code)
For severe jamming, use only code track

transfer bus, which services the receiver subsystem, is visible in this diagram. The receiver signal processing software is contained in the core memory. The memory and CPU form the basic CAPS-4 architecture; the 1553A interface is an addition mode for GPS.

Figure 11 shows a software block diagram of the receiver processor software. Functionally the software includes the sequence of operations shown in table 2. The system is initialized and calibrated with test signals, C/A acquisition of four SV's is accomplished, the SV's are tracked, the data is synchronized and demodulated, GPS time is decoded, the code generator slewed for the C/A to P handover, P-code tracking of code and carrier

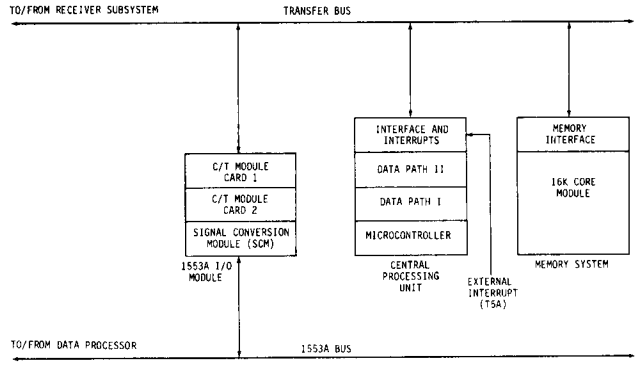

Figure 10. Receiver Controller Components.

is maintained, and, under severe jamming, the system reverts to noncoherent code tracking.

In figure 11, one of the inputs from the navigation data processor is velocity aiding data. This data is combined with the processed receiver measurements as code and carrier vco command data. The velocity aid data basically adds the IMU velocity measurements to the vco's so that the vco's must track only the residual error in the velocity input. This topic is covered in detail in a later paper.

Figure 11 also shows the operational separation of the processing into fast (5 ms), slow (20 ms), management (100 ms), background, and 1553A I/O operations. The basic interrupt rate is every 5 ms and is derived from the system frequency synthesizer. This interrupt identifies instants in time when the code generator positioning is accurate within a few nanoseconds. It is common to all SCP's, so that time-of-arrival differences can be read simultaneously for all channels.

The 5-ms loop is used basically as the sample rate for a 200-Hz predetection if bandwidth. Following initial acquisition and assuming inertial aiding, 20-ms samples are used corresponding to the 50-Hz data rate. The data, however, is not mutually synchronous between SV's so the 5-ms loop maintains control to determine the occurrence of 20-ms samples for each channel.

The 20-ms loop is basically used for delay lock loop (code) tracking and for code generator control and code position computation. The 100-ms loop basically checks the mode in which the faster loops are operating. For example, it will cause code tracking to switch from coherent to noncoherent tracking when the J/S is high. The background tasks, which are basically data framing and parity check functions, are operated as time is available after operation of the 5-, 20-, and 100-ms loops.

SUMMARY

This paper describes the mechanization of the GPS/GDM receiving subsystem. The emphasis is on the hardware description, but design rational and software mechanizations are discussed where applicable. A brief GDM/GPS system description was given with detailed description of the rf unit, which basically provides rf-to-if conversion; the signal channel processor, which provides the analog/digital interface from if to the receiver processor; and the receiver processor which contains the acquisition, tracking, and demodulation algorithms. The GDM/GPS equipment provides a versitile, extremely flexible test receiver, which under software control, can be configured to represent different levels of sophistication and performance of GPS receivers.

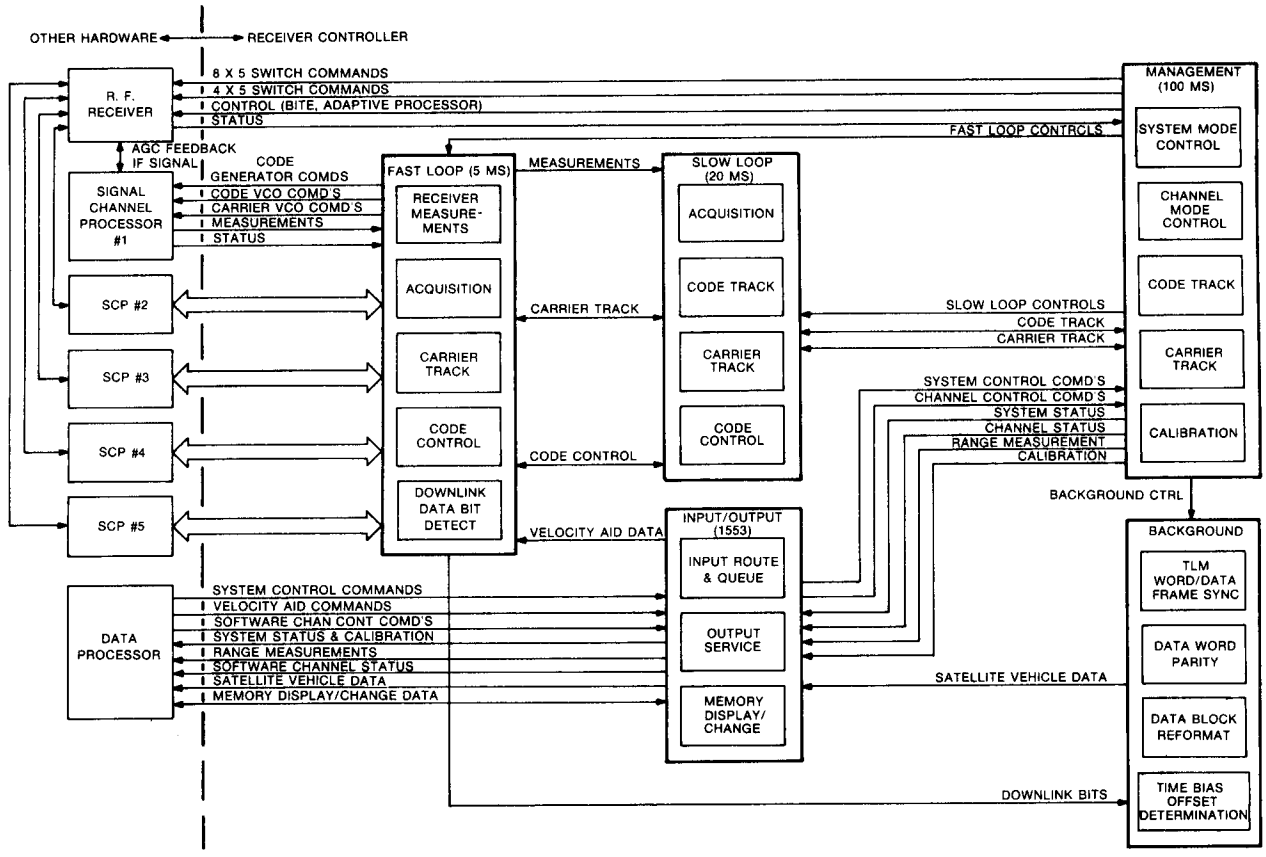

Figure 11. Program Data/Control Flow.

A GPS USER EQUIPMENT PERFORMANCE EVALUATOR (GPSE)

Bernard Cooper

ITT Defense Communication Division
Nutley, New Jersey

ABSTRACT

The GPSE is currently under development and will provide the means for real time simulation of the total dynamic environment experienced by a GPS User Equipment in actual operation. This simulation includes the generation of:

- GPS RF Signals
- Jammer RF Signals
- White Gaussian Noise
- GPS Navigation Data
- On-board Sensor Signals (i.e. IMU and altimeter)
- Path loss and Antenna Pattern

As part of the simulation, error models for various functions and phenomena including IMU, altimeter, Ionospheric and tropospheric delay, gravity, anomaly, ephemeris, and clock errors will be included.

The simulator precisely couples the changes in RF signals (i.e. doppler) to the physical dynamics of the system (i.e. User, satellite and jammer motion) including lever arm effects.

Provision is also being made to collect, use and analyze performance data.

The GPSE is currently planned to simulate four GPS Satellite RF channels with provision for future addition of a fifth channel. Five RF jammer channels will also be provided. The entire simulation is under real time software control, utilizing as the input precomputed data defining the user flight profile.

VELOCITY AIDING OF NONCOHERENT GPS RECEIVER

R. W. Carroll
W. A. Mickelson

Collins Avionics Division, Rockwell International
Cedar Rapids, Iowa

ABSTRACT

Operation of a GPS receiver in the face of heavy interference generally implies noncoherent code-tracking, since carrier phase lock is typically lost. In this configuration, velocity aiding of the noncoherent code-tracking loop can permit a significant code-loop bandwidth reduction. As a consequence, useful code tracking and navigation performance are retained. However, the reduction of code-loop bandwidth results in long correlation time for the errors in pseudorange measurements extracted from the code loop. Moreover, these errors are heavily correlated with the errors in the velocity aid.

This paper discusses the system impact of velocity-aid/measurement error correlation from both navigation and code-loop tracking viewpoints. A possible system instability is avoided through (1) development of a compensation element and (2) proper selection of Kalman filter response characteristics with respect to GPS code-loop dynamics.

INTRODUCTION

Velocity aiding of a GPS receiver with INS-derived velocity can permit significant reduction of the bandwidth of the receiver tracking-loops, since the burden of tracking vehicle dynamics is thereby removed. This bandwidth reduction implies a corresponding increase of receiver resistance to rf interference.

Typically, navigation errors induced by the inertial measurement unit are estimated by a Kalman filter through processing of range measurements obtained from a code-tracking loop in the GPS receiver. If the best estimate of vehicle velocity (computed velocity corrected by the Kalman error estimate) is used for receiver aiding, certain benefits are attained such as reduced sensitivity of GPS code tracking to INS errors. However, if the overall feedback of Kalman velocity corrections to the GPS measurements is not accounted for, system instability can result.

The essence of this potential instability problem lies in two factors:

1. The Kalman error-state vector does not model code-loop dynamics, ie, all range measurements are assumed to be independent.
2. The code-loop error states are directly observed in the Kalman measurements, and the differential equations they satisfy are coupled through line-of-sight geometry to the INS velocity-error states, which are modeled by the Kalman filter.

Thus, there is a gross discrepancy between the error dynamics assumed by the Kalman filter and those which, in fact, exist. It is tacitly assumed that the rf interference is high enough that carrier tracking cannot be maintained, and velocity aiding of the code loop must come solely from the INS. (Normally, INS aiding is applied to the carrier-tracking loop which in turn aids the code loop.)

Investigation of single axis models of the GPS/INS Kalman filter interaction with the GPS receiver code loop, when rate aiding, reveals that a positive feedback loop exists within the system structure. A detailed analysis of the problem shows that the overall system response is either unstable or very underdamped depending upon the response time of the Kalman filter with respect to the code-loop response time. A compensation loop which yields a well damped overall system response has been defined and analyzed. Implementation of the compensation loop is confined to the GPS navigation computer software.

This paper treats two different Kalman filter models. One model corresponds to a third-order vertical axis Kalman filter whereas the second model represents a fourth-order lateral axis Kalman filter. In either case, the linear system model uses steady-state Kalman filter gains to investigate the closed loop system stability and response characteristics. The discussion below relates primarily to the vertical axis model with brief paragraphs to indicate how the corresponding lateral problem differs from the vertical problem.

The vertical axis of the GPS/INS mechanization uses the GPS pseudorange data to stabilize the inherently unstable INS vertical loop. This stabilization is implemented by applying the Kalman error estimates as control updates to the whole-value vertical navigation variables (position, velocity, acceleration). Figure 1 depicts a generalized information flow diagram for the vertical

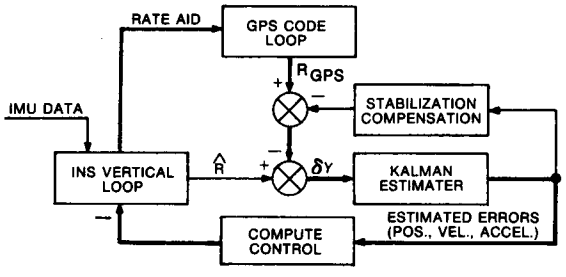

Figure 1. Generalized Information Flow Diagram.

axis. It shows the Kalman filter error estimates being fed back as closed loop control to stabilize the INS vertical loop. The resulting vertical velocity is used to rate-aid the GPS code loop. The GPS position (R_{GPS}) is then compared with the computed position to obtain the Kalman filter observation (δy). The heavy black line in

figure 1 traces the system loop which has positive feedback. It should be noted that this loop exists only if the Kalman filter error estimates are used as components of rate aid to the GPS code loop.

The existence of a positive feedback loop within a larger overall system may cause the total system to be unstable. In this case, analysis shows that the system is unstable when operating with a code loop whose noise bandwidth (B_L) is 0.01 Hz and a Kalman filter of conventional design. This establishes a requirement to (1) restructure the rate aid and the INS vertical loop stabilization or (2) develop a compensation loop to effectively stabilize the closed loop vertical axis described above (figure 1), or (3) augment the error state vector to correctly model the interaction. The decision to develop a compensation loop was based upon the following considerations.

- Desire to minimize the effects of rate-aid error upon resistance to rf interference.
- Desire to retain the GPS/INS/altimeter information processing entirely within the Kalman filter, thus maintaining a logically simple system definition and avoiding a separate INS/altimeter loop.
- Impracticality of a major extension to the error-state vector.

GENERALIZED ANALOG MODEL DEVELOPMENT

The general components of the type of system under discussion are:

1. A set of continuous, linear differential equations that describe the dynamics of the actual error states.
2. A discrete Kalman filter that periodically samples the error states and applies impulsive control to some of the states based usually upon an incomplete model of the actual errors and their dynamics.

Suppose the actual error-state vector, x, satisfies

$$\dot{x}(t) = A\,x\,(t) + DW\,(t) \tag{1}$$

where W is generally a random forcing vector. If the Kalman discrete observation is:

$$y^*\,(t) = Mx^*\,(t)\ , \tag{2}$$

then the closed-loop system obeys

$$\dot{x}(t) = Ax(t) - B'Mx^*(t) + DW(t)\ . \tag{3}$$

The term, $B'Mx^*(t)$, is the impulsive control applied to the error states. M is the measurement matrix and describes (via equation (2)) the actual observations. B' contains the Kalman filter steady-state* gain matrix. Typically, some components of B' will be zero, corresponding to unmodeled states. If the response times of the overall system are long compared to the Kalman filter sampling and control time interval, T, equation (3) may be approximated by:

$$\dot{x}(t) = \frac{(A-B'M)}{T}\,x(t) + DW(t)\ . \tag{4}$$

To be more specific, let λ_m denote the eigenvalue of A-B'M/T with largest magnitude. Then, experience has shown that if

$$\lambda_m < 0.1(2\pi/T), \tag{5}$$

equation (4) is an accurate approximation.

Note that stability of the analog model requires that the eigenvalues of A-B'M/T have negative real parts.

*Conditions for steady-state gain are derived in the Appendix.

This is an adequate stability check when equation (5) is satisfied.

It is shown in the Appendix that an exact stability check can be made based on the polynomial:

$$g(z) = \det\left[z(I+B'M) - \exp(AT)\right]\ . \tag{6}$$

For each z_i, such that $g(z_i) = 0$, it is required that $|z_i| < 1$. Thus, $g(z)$ is the characteristic equation for the system described by equation (3), when viewed as a sampled-data system. $|z_i| < 1$ guarantees that the solution of equation (3), for bounded input, will be bounded at the sample times. It should be emphasized that B', in the above results, is the discrete steady-state gain matrix for the Kalman filter. From this point forward, the equivalent analog gain,

$$B = B'/T\ , \tag{7}$$

will be used.

It will be convenient to partition the overall system of figure 1 into three parts:

1. The basic nav-error dynamics with Kalman-filter control.
2. The GPS code-tracking loop.
3. The compensation block.

The corresponding analog models are developed in the next sections.

ANALOG MODEL FOR NAV ERRORS AND KALMAN FILTER

Define the vertical axis error states as:

$$x = \begin{bmatrix} x_1 \\ x_2 \\ x_3 \end{bmatrix} = \begin{bmatrix} \text{Altitude error} \\ \text{Vertical velocity error} \\ z\text{-accelerometer error} \end{bmatrix}\ . \tag{8}$$

Then, it is well known that x satisfies the basic differential equation

$$\dot{x} = \begin{bmatrix} 0 & 1 & 0 \\ 2g/R & 0 & 1 \\ 0 & 0 & 0 \end{bmatrix} x \tag{9}$$

where g is the acceleration of gravity and R is earth radius. Random forcing functions are not included in (9). Considering equation (9) to be the system (rate-aid link in figure 1 broken), the measurement matrix is:

$$M_{vert} = \begin{bmatrix} 1 & 0 & 0 \end{bmatrix} \tag{10-a}$$

and the analog Kalman gain is

$$B_{vert} = \begin{bmatrix} B_R & B_V & B_a \end{bmatrix}^T \tag{10-b}$$

Thus, from equation (4), the dynamics of the vertical axis nav errors and Kalman filter, exclusive of any rate-aiding feedback, satisfy

$$\dot{x} = (A - B_{vert}M_{vert})x = \begin{bmatrix} -B_R & 1 & 0 \\ (2g/R) - B_V & 0 & 1 \\ -B_a & 0 & 0 \end{bmatrix} x \tag{11}$$

The characteristic equation corresponding to (11) is:

$$\det\left[SI - A + B_{vert}M_{vert}\right] = S^3 + B_R S^2 + (B_V - \frac{2g}{R})S + B_A \tag{12}$$

The eigenvalues for the vertical axis are the roots of (12). Given values for the Kalman gains, these roots can be found and (12) can be rewritten*

$$g_{vert}(s) = (S + \tfrac{1}{\tau})\,(S^2 + 2\xi\omega_n S + \omega_n^2)\ . \tag{13}$$

*Typically, the Kalman steady-state gains will yield one real pole and a complex pole pair.

Subsequent results for the overall system performance are discussed in terms of the parameters r, ξ, and ω_n.

The block diagram corresponding to (11) is shown in figure 2. The forcing function, ϵV_z, corresponds to

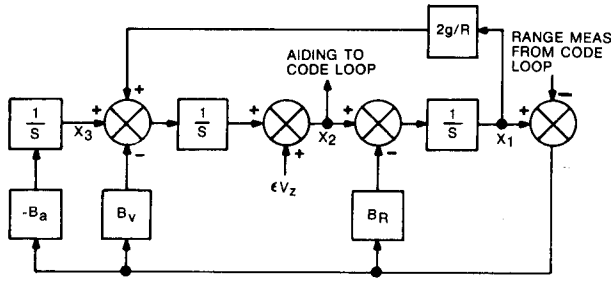

Figure 2. Vertical Axis Analog Equivalent.

velocity errors induced by unmodeled INS errors such as accelerometer scale-factor and misalignment errors, and will be discussed later.

For the lateral axis, the nav error states are position error, velocity error, platform tilt, and gyro drift. It can be shown that the characteristic equation for a lateral axis is given by

$$g_{lateral}(s) = S^4 + B_R S^3 + (B_V + \frac{g}{R}) S^2 + g(B_\phi + \frac{B_R}{R}) S + g B_D \qquad (14)$$

and typically has two pairs of complex roots (eigenvalues). Given values for the four filter gains (14) can be rewritten

$$g_{lateral}(s) = (S^2 + 2\xi_1 \omega_{n1} S + \omega_{n1}^2)\ (S^2 + 2\xi_2 \omega_{n2} S + \omega_{n2}^2) \qquad (15)$$

CODE LOOP MODEL

The GPS receiver code loop operating in a noncoherent mode is modeled by a linear second order transfer function (figure 3). The dynamics of the transfer

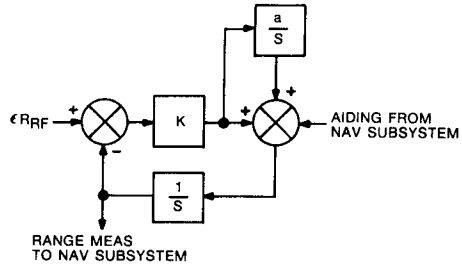

Figure 3. GPS Noncoherent Code-Tracking Loop.

function are determined by the gains "K" and "a." The gain K is dependent upon the total input power (signal-plus-noise power), whereas the gain a is fixed. The characteristic equation of the code loop is:

$$s^2 + Ks + Ka = 0 = s^2 + 2\xi_c \omega_c s + \omega_c^2 \qquad (16)$$

It should be noted that increasing the gain K results in an increase in both the loop damping ratio (ω_c) and the natural frequency (ξ_c). Note that an input for rf interference, ϵR_{RF}, is included in figure 3.

OVERALL ANALOG MODEL AND COMPENSATION

The overall analog model for the vertical axis, including the compensation block, is shown in figure 4. The structure of the velocity aid compensation was motivated as follows:

1. The system instability occurs when Kalman filter error estimates, acting through rate aiding, affect the GPS pseudorange error (δR_{GPS}).
2. By duplicating the open loop transfer function from the Kalman error estimate X_{14} to the GPS pseudorange error (δR_{GPS}), the destabilizing effect can be removed.
3. The open loop transfer function is

$$\frac{\delta R_{GPS}}{X_{14}} = \frac{1}{s^2 + Ks + Ka} \qquad (17)$$

The gain K is variable. Therefore, the destabilizing effect can only be partially removed.

4. By formulating the compensation loop to have the open loop transfer function

$$\frac{X_{13}}{X_{14}} = \frac{1}{s^2 + \kappa s + \kappa a} \qquad (18)$$

the compensation loop transfer function has the desired form.

DISCUSSION OF ERROR SOURCES

First consider the principle error sources exciting this system. These error sources can be classified as either GPS receiver errors or IMU-induced errors. The GPS receiver errors include clock errors and pseudorange errors caused by rf interference. The effect of rf interference is modeled as a white noise input to the code loop (ϵR_{RF} in figure 4). The magnitude of the rf noise power input is considered to be a design variable. The design objective is to maximize the level of rf interference at which system code-loop lock is maintained.

The principle errors introduced by the IMU are the acceleration errors caused by the accelerometer scale factor and misalignment errors and by the computer to platform misalignment angle $\bar{\psi}$. The acceleration error may be written in vector form as:

$$\epsilon A = \begin{bmatrix} \epsilon K_x & M_{xz} & -M_{xy} \\ -M_{yz} & \epsilon K_y & M_{yx} \\ M_{zy} & -M_{zx} & \epsilon K_z \end{bmatrix} \bar{A} + \bar{A} \times \bar{\psi} \qquad (19)$$

where:

ϵK_i = the accelerometer scale factor error ($i = x, y, z$),
M_{ij} = the misalignment of the accelerometer input axis i about the j axis,
$\bar{A}$ = the total acceleration vector, and
$\bar{\psi}$ = computer to platform misalignment angle.

Let the acceleration vector be:

$$\bar{A} = \begin{bmatrix} A_X & 0 & 0 \end{bmatrix}^T \qquad (20)$$

Then

$$\epsilon\bar{A} = A_X \begin{bmatrix} \epsilon K_X \\ -(M_{yz} + \psi_z) \\ (M_{zy} + \psi_y) \end{bmatrix} \qquad (21)$$

By integrating both sides of this equation, we obtain

$$\epsilon V = V_X \begin{bmatrix} \epsilon K_X \\ -(M_{yz} + \psi_z) \\ (M_{zy} + \psi_y) \end{bmatrix} \qquad (22)$$

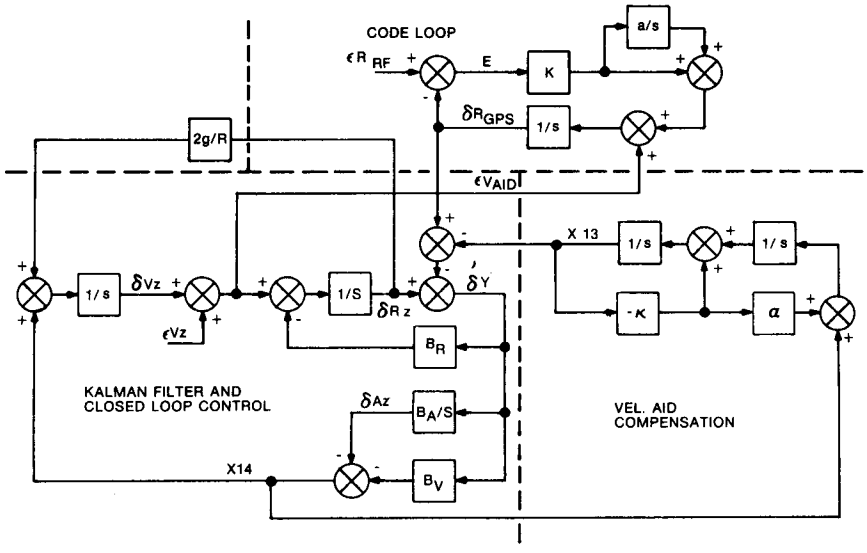

Figure 4. Overall Vertical Channel Analog Model With Closed Loop Control, Velocity Aiding and Velocity Aid Compensation.

Typical values of the error parameters are as follows:

ϵK_i ~ 2×10^{-4} to 10^{-3}
M_{ij} ~ 2×10^{-4} to 10^{-3} radians
ψ_i ~ 10^{-3} to 5×10^{-3} rad for the pure inertial IMU
ψ_i ~ 10^{-4} to 5×10^{-4} rad for the Kalman aided IMU

Assuming that the effects of M_{ij} and ψ_i are additive, the magnitude of the velocity error then becomes

$$|\epsilon V|_{\text{closed loop}} = V_X (1.5 \times 10^{-3}) \quad (23)$$

and

$$|\epsilon V|_{\text{open loop}} = V_X (6 \times 10^{-3}) \quad (24)$$

For the above assumed values, the velocity error forcing function $|\epsilon V|$ is four times larger for the open loop case than for the closed loop case.

Assume that the velocity varies as

$$V_X = V_o \sin \beta t = 200 \sin \beta t \text{ m/s} \quad (25)$$

Then $\epsilon V = .3 \sin \beta t$ for closed loop operation (26)

and $\epsilon V = 1.2 \sin \beta t$ for open loop operation. (27)

PERFORMANCE EVALUATION CRITERIA

Several performance parameters have been identified by which candidate system designs are compared. The most important parameters are tabulated as follows:

$\left\lvert \frac{\delta R_{GPS}}{\epsilon V_z} \right\rvert$ MAX	The maximum amplitude of the transfer function from IMU velocity error to pseudorange error.
$\left\lvert \frac{\delta R_{GPS}}{\epsilon R_{RF}} \right\rvert$ RMS	The RMS value of pseudorange error response to a white noise input ϵR_{RF} whose 2-sided PSD is $1 M^2/Hz$.
$\left\lvert \frac{\delta R_{GPS}}{\epsilon V_{STEP}} \right\rvert$ Peak	The peak value of the pseudorange time response to a unit step in IMU velocity error.
$\left\lvert \frac{\delta R_z}{\epsilon V_z} \right\rvert$ MAX, $\left\lvert \frac{\delta R_z}{\epsilon R_{RF}} \right\rvert$ RMS, and $\left\lvert \frac{\delta R_z}{\epsilon V_{STEP}} \right\rvert$ Peak	Similar to the above parameters with pseudorange error replaced by navigation error δR_z.

The performance parameters relating to pseudorange errors are considered to be the most important in evaluating candidate system designs. These parameters are used to predict the code-loop tracking capability in the presence of rf noise.

The navigation error performance parameters indicate the navigation error response to the indicated inputs. However, in using these performance parameters, it should be recognized that several unobservable errors such as residual ionospheric errors and tropospheric errors and receiver calibration errors will further reduce the navigation accuracy. Also, the navigation errors due to the system error inputs are small for the GPS/INS NAV system as compared to the pure INS navigation errors which result when the code-loop tracking is lost. Therefore, it is concluded that the performance parameters relating to pseudorange errors are more important than those relating to navigation accuracy.

SOLUTION APPROACH

The design of the closed loop rate-aided system shown in figure 4 is divided into three parts as follows:

- Select the code-loop bandwidth
- Design the velocity aid compensation function
- Determine the Kalman filter transfer function which optimizes the system performance

The code-loop bandwidth is selected to minimize the C/No ratio for which code-loop lock is maintained in the presence of a rate-aid acceleration error. Figure 5 shows the results of a computer study. Four curves are shown to illustrate the code-loop tracking capability in the presence of acceleration (acceleration error for the velocity aided code loop). The generation of these curves requires a computer program simulation and is outside

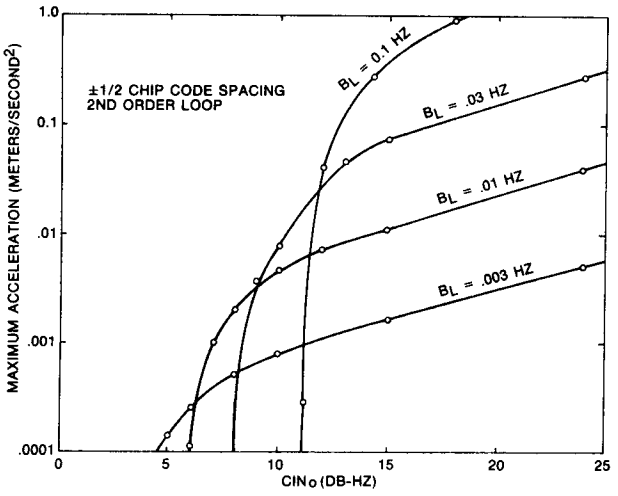

Figure 5. Code Delay-Lock Loop Bandwidth Trade-off.

the scope of this paper. However, the results are presented to illustrate their use in selecting the code-loop bandwidth. Suppose the maximum acceleration error is 0.01 m/s. Figure 5 shows that code track is maintained at (1) C/No = 14 dB - Hz for B_L = 0.01 Hz; (2) C/No = 10.5 dB - Hz for B_L = 0.03 Hz; and (3) C/No = 12 dB - Hz for B_1 = 0.1 Hz. The code-loop bandwidth is, therefore, chosen as B_L = 0.03 Hz. The ideal bandwidth, B_L, could be further refined by determining curves for additional bandwidths in figure 5. However, this is probably not warranted since the acceleration error is not accurately known.

Assuming a compensation transfer function of the form located as shown in figure 4, performance parameters for perturbations in B, ξ_B, and ω_B were evaluated.

$$C_{(s)} = \frac{B}{s^2 + 2\xi_B\omega_B s + \omega_B^2} = \frac{B}{s^2 + \kappa s + \kappa a} \qquad (28)$$

It was found that the performance is quite insensitive to variations of B from 0.8 to 1.2. Variation of κ from $\kappa = K_0$ to $3K_0$ (corresponds to gain variation of code loop) revealed that the system is unstable with $\kappa = 3K_0$. The obvious design choice is to set

$$C(s) = \frac{1}{s^2 + 2\xi_c\omega_c s + \omega_c^2} \qquad (29)$$

where ω_c and ξ_c are the code-loop values under maximum interference.

The Kalman filter is assumed to be a 3-state filter for the vertical axis with states corresponding to position, velocity, and acceleration error. By varying the Kalman gains, ie, the Kalman filter transfer function, the closed loop system response to specified inputs is changed. The objective of the final stage of the design effort is to identify the Kalman filter which yields the best system response.

RESULTS

For this study, a code-loop bandwidth B_L = 0.01 Hz was initially assumed. The first design efforts were to find the velocity aid compensation which yielded the best performance with a Kalman filter of conventional design (no special consideration given to rate-aid feedback). These efforts were successful in stabilizing the vertical loop behavior. However, the pseudorange error sensitivity to IMU velocity error was judged to be too great. It was concluded that a wider bandwidth code loop was necessary for the expected acceleration and velocity errors. Finally, the Kalman filter response characteristic was modified to find the filter giving the best navigation performance while maintaining near minimal code-loop error.

The results obtained in this study are presented below in two groups. The first group relates to a code loop with B_L = 0.01 Hz and Kalman filter gains for the conventional design. The results primarily concern the design of the velocity aid compensation block.

The second group of results relates to a code loop with B_L = 0.02 Hz and primarily concerns the design of the Kalman filter transfer function to yield the best performance.

RESULTS WITH CODE LOOP B_L = 0.01 Hz

The first studies conducted were for a code loop with B_L = 0.01 Hz and a conventional Kalman filter. The form of compensation was that shown in figure 4. The closed loop response of the system to IMU velocity errors (ϵV_Z) was determined and plotted. Figure 6 shows the frequency response of pseudorange error

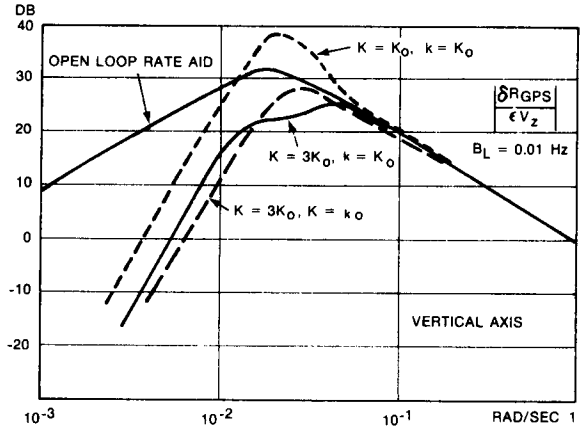

Figure 6. Code-Loop Response to ϵV_Z (B_L = 0.01 Hz).

(δR_{GPS}) to ϵV_Z. Since the code-loop gain K may increase by a factor of 3 or 4 from the minimum design value (κ_0 = .0266), the effects of this variation were investigated. Curves are shown with combinations of the code-loop gain (K) and the velocity aid compensation (κ) equal to K_0 or $3K_0$. The combinations of runs show that the compensation gain (κ) should not significantly exceed the code-loop gain (K). Since the code-loop gain is an unknown value to the navigation computer, the choice of $\kappa = K_0$ must be made.

Figure 6 shows a peak pseudorange error (δR_{GPS}) of 38.7 dB or 86 metres for a unit velocity error input. Assuming an actual sinusoidal velocity error of 0.2 m/s, the maximum pseudorange error is 17.2 metres.

Figure 7 shows the result of computer simulation which illustrates the required reduction of pseudorange variance due to rf noise in order to maintain code-loop track in the presence of a code-loop standoff. It is apparent from figure 7 that a loop standoff of 17 metres severly limits the tracking capability in the presence of

Table 1. Summary of Performance Results For Vertical Loop.

RUN	CODE LOOP	KALMAN FILTER ω_n	KALMAN FILTER ξ	KALMAN FILTER $1/\tau$	$\left\|\frac{\delta R_{GPS}}{\epsilon V_Z}\right\|$ MAX	$\left\|\frac{\delta R_Z}{\epsilon V_Z}\right\|$ MAX	$\left\|\frac{\delta R_Z}{\epsilon R_{RF}}\right\|$ RMS	NAV COST (m)	VEL AID COMPENSATION	COMMENTS
1	B_L = 0.02 Hz	.024	0.49	.024	37.8	51.7	.193	11.2	1.2 X code loop	Conventional design
2	B_L = 0.02 Hz	.037	1.0	.01	29.9	32.5	.190	8.1	1.2 X code loop	
3	B_L = 0.02 Hz	.037	1.0	.005	28.4	32.8	.186	8.1	1.2 X code loop	
4	B_L = 0.02 Hz	.037	1.0	.02	31.7	31.2	.196	7.9	1.2 X code loop	
5	B_L = 0.02 Hz	.018	1.0	.01	27.3	42.5	.170	9.5	1.2 X code loop	
6	B_L = 0.02 Hz	.018	1.0	.005	25.4	43.0	.161	9.5	1.2 X code loop	
7	B_L = 0.02 Hz	.037	1.0	.005	38.9	59.5	.250	13.5	No comp	
8	K = 4 X run 1	.037	1.0	.005	6.1	19.4	.226	6.8	No comp	High-gain code loop
9	K = 4 X run 1	.037	1.0	.005	5.6	22.3	.200	6.7	Same run 1	High-gain code loop
10	B_L = 0.02	.018	1.0	.005	28.1	53.2	.182	11.5	No comp	
11	B_L = 0.02	.037	1.0	.005	29.4	34.5	.193	8.4	1.0 X code loop	
12	B_L = 0.03	.030	1.0	.01	18.1	28.4	.211	7.7	1.0 X code loop	Note B_L = 0.03
13	B_L = 0.02	.037	1.0	.005	18.8	34.5	.193	8.4	None	Pure INS velocity aid

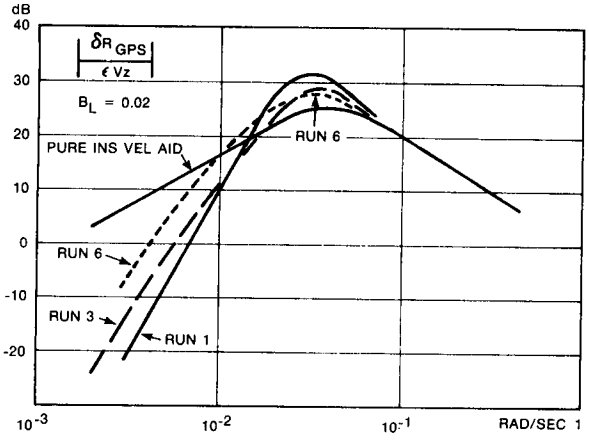

Figure 8. Code-Loop Response to ϵV_Z (B_L = 0.02 Hz).

aircraft maneuvers. Still higher frequency errors are expected from high performance aircraft.

Finally, the δR_{GPS} time response to a step in ϵV_Z was obtained for the system models of runs 11 and 13. The results show that the code-loop error is 12.1 metres for the pure INS velocity aid of run 13 whereas it is 11.2 metres for run 11. While this appears to be only a small difference, the magnitude of the forcing function in run 13 is expected to be four times larger with a corresponding increase in peak code-loop error.

CONCLUSIONS AND RECOMMENDATIONS

The principle advantage of using Kalman filter error estimates in computing the velocity aid is that a reduced code-loop bandwidth, B_L, is justified. This results in the code loop maintaining lock in the presence of greater rf noise than would otherwise be possible.

The utilization of Kalman filter error estimates to improve the rate-aid commands to the receiver can cause system instability. This instability can be avoided by designing the Kalman filter response time to be long compared to the code-loop time constants. However, slowing the filter response time increases the navigation error.

By introducing a velocity aid compensation, it is possible to retain a moderately fast responding Kalman filter and still achieve excellent system stability. Results have shown that the velocity aid compensation should correspond to the transfer function given by equation (18).

By using a velocity aid compensation which matches the code-loop dynamic characteristic, the effect of Kalman filter rate-aid components on the pseudorange measurement is computed. Subtracting this value from the measured pseudorange then yields a modified pseudorange that would result from a pure INS velocity aid. Hence, the observation available to the Kalman filter is unaffected by previous observations. By comparing runs 11 and 13 in table 1, we note that the ϵR_Z response to error sources ϵV_Z and δR_{RF} is unchanged. This is a consequence of the velocity aid compensation exactly canceling the effects of Kalman filter corrections on the pseudorange measurement.

This study was conducted on the basis that the Kalman filter gains are constant. The real 3-axis system will not result in constant gain although the characteristic response times probably will not vary by more than a factor of two. These response times will be a complex function of aircraft dynamics and the GPS line-of-sight (LOS) geometry. The inclusion of the stability

compensation block will provide extra stability margins in the three dimensional time variable gain environment.

Much of the above analysis was conducted with B_L = 0.02 Hz. However, as indicated by equation (26), the velocity aid error will probably be modestly higher than the assumed 0.2 m/s. The actual receiver code loop is currently designed with B_L = 0.03 Hz, and is thus less sensitive to velocity aid errors. One additional run was made to evaluate the system vertical axis performance for the following system design:

Code loop:
B_L = 0.03 Hz (ω_c = .0565 rad/s, ξ_c = .707)
or (K = .08 s^{-1}, a = .04 s^{-1})

Kalman filter:
ω_n = .03 rad/s, ξ = 1.0, $1/\tau$ = 0.01 s^{-1}
or B_R = .07 s^{-1}, B_V = 1.503 x 10^{-3} s^{-2},
B_A = 9 x 10^{-6} s^{-3}.

Velocity Aid comp:

$$\frac{X_{13}}{X_{14}} = \frac{1}{s^2 + \kappa s + \kappa a} \quad \text{where } \kappa = .08\ s^{-1},\ a = .04\ s^{-1} \tag{32}$$

The results are included as run 12 of table 1. Probably the most significant result of this run is the reduced sensitivity to code-loop error to ϵV_Z.

APPENDIX

STEADY STATE KALMAN FILTER GAINS

The discrete Kalman filter is described by the following recursion:

$$P^*_n = \Phi_{n-1,n} P_{n-1} \Phi^T_{n-1,n} + Q_{n-1,n} \tag{A-1}$$

$$B'_n = P^*_n M^T_n (M_n P^*_n M^T_n + V_n)^{-1} \tag{A-2}$$

$$P_n = (I - B'_n M_n) P^*_n \tag{A-3}$$

where P* denotes covariance before measurement processing, B' is the discrete processing gain, P denotes covariance after measurement processing and n denotes iteration number (time index). Φ describes the state transition from previous to current iteration and Q is the covariance of state forcing noise as integrated over the previous interval.

In steady state, the time subscripts may be dropped (n and n-1) since then $P_n = P_{n-1}$, $P^*_n = P^*_{n-1}$, etc. Thus, from equations (A-1), (A-2), and (A-3), the nonlinear matrix equation that must be satisfied at steady state is:

$$\Phi\left[P^* - P^* M^T (MP^* M^T + V)^{-1} MP^*\right] \Phi^T + Q - P^* = 0 \tag{A-4}$$

It is assumed in (A-4) that the system matrix for the error dynamics is not time-varying, ie, that Φ = exp(AT) is valid, and that the system forcing noise is time-stationary (Q is constant).

Let P* be the positive-definite matrix that satisfies (A-4). Then, the steady-state gain for the Kalman filter is:

$$B' = P^* M^T (MP^* M^T + V)^{-1}. \tag{A-5}$$

For the results in this paper, (A-4) was solved on the computer using a modified Newton-Raphson technique.

CLOSED LOOP DISCRETE KALMAN STABILITY REQUIREMENTS

Let x(n) be the closed-loop system state vector at the nth sample time. Then, the following recursion implicitly relates x(n+1) to x(n) with no forcing.

$$x(n+1) = \Phi x(n) - B'M\, x(n+1) \tag{A-5}$$

where Φ = exp(AT) and T is the sampling interval. Taking the z-transform of (A-5) yields

$$\left[I + B'M\right]\left[z\, X(z) - z x(0)\right] = \Phi X(z)$$

so that X(z) satisfies

$$\left[z\,(I + B'M) - \Phi\right] X(z) = z\left[I + B'M\right] x(0) \tag{A-6}$$

where x(0) is the initial value of the state vector.

Clearly,

$$g(z) = \det\left[z\,(I + B'M) - \Phi\right] \tag{A-7}$$

is the characteristic equation for the discrete system of (A-5). Moreover, for x(n) to be bounded for all n, it is necessary that

$$|z_i| < 1 \tag{A-8}$$

for all z_i such that

$$g(z_i) = 0. \tag{A-9}$$

This is a direct consequence of the fact that each component of x(n), $x_j(n)$, can be expressed in the form

$$x_j(n) = \sum_{i=0}^{p} a_i z_i \tag{A-10}$$

where p is the order of g(z).

REFERENCES

"Critical Design Review of AFAL GDM/GPS User Equipment -- Receiver Algorithm Performance Analysis," Collins Avionics Division, Rockwell International, Cedar Rapids, Iowa; December 1976.

Pitman, George R., Inertial Guidance, New York, John Wiley and Sons, 1962

Sage, Andrew P., Optimum Systems Control, Englewood Cliffs, New Jersey, Prentice Hall, 1968.

Tou, Julius T., Digital and Sample Data Control Systems, New York, McGraw-Hill, 1959.

LIMITATIONS ON GPS RECEIVER PERFORMANCE IMPOSED BY CRYSTAL-OSCILLATOR g-SENSITIVITY

Joseph M. Przyjemski
Philip L. Konop

The Charles Stark Draper Laboratory, Inc.
Cambridge, Massachusetts 02139

ABSTRACT

The sensitivity of crystal reference oscillators to vibrations and other dynamics limits tracking performance in Navstar GPS radio navigation receivers used in tactical aircraft. Frequency variations resulting from this sensitivity impose a lower bound on receiver bandwidths, and consequently limit antijam (A/J) capability.

An analysis is performed which illustrates relationships between GPS carrier-tracking-loop bandwidth requirements and g-sensitivity of an oscillator in various dynamic environments. The results show that the level of susceptibility of frequency changes to g-loading in state-of-the-art crystal oscillators is unacceptable for noise bandwidths in the 1-Hz range.

It is proposed that dynamic compensation of the effects of g-sensitivity be performed. Thus, characterization of this parameter is required for its inclusion in a suitable oscillator model. A test system is described which generates the characteristics of the oscillator g-sensitivity in terms of its frequency response.

INTRODUCTION

The crystal oscillator used in Navstar GPS receivers limits the minimum obtainable carrier-tracking-loop bandwidths because of oscillator frequency sensitivity to shock, vibration, and acceleration. This sensitivity, in turn, limits the ultimate antijam (A/J) capability of the receivers under tactical and strategic aircraft and missile dynamic conditions.

Because of oscillator sensitivity to these acceleration forces, a tracking loop with a low bandwidth may lose lock under dynamic conditions. For example, present GPS-qualified crystal oscillators have typical fractional frequency sensitivities of 1×10^{-9}/g of acceleration along the most sensitive crystallographic axis. Given a simulated tactical dynamic input of 10 g/s lasting 0.6 s, a tracking noise bandwidth of 16.6 Hz is required to ensure a maximum tracking error of 0.1 rad. However, to provide maximum A/J capability, receiver carrier-tracking bandwidths in the 1-Hz region are desired. The resulting tracking error is shown to exceed the loss-of-lock threshold of the tracking loop.

The severity of this problem is compounded by the inadequacy of mechanical isolators to provide dynamic attenuation under conditions of constant acceleration or low vibration frequencies. As will be shown, it is at these frequencies that g-induced tracking-loop error is greatest. Since it is unlikely in the near future that the g-sensitivity of the crystal oscillator will be significantly diminished, alternative dynamic-compensation techniques must be implemented if these oscillators are to be used in GPS-type receivers. This paper analytically assesses the magnitude of the problem and describes a technique for measuring the g-sensitivity parameter.

VIBRATION-INDUCED PHASE ERROR

Vibrations transmitted to the resonator in a crystal reference oscillator cause deviations in its nominal frequency. The actual output frequency can be written as

$$f(t) = f_o + \Delta f_o(t) \tag{1}$$

where

$f(t)$ = instantaneous frequency (Hz).

f_o = undisturbed center frequency (Hz).

$\Delta f_o(t)$ = vibration-induced frequency deviation (Hz).

For the purpose of this analysis, it is assumed that the oscillator g-sensitivity is independent of both the amplitude and frequency of vibration. Frequency deviation is given by

$$\Delta f_o(t) = S_g f_o a(t) \tag{2}$$

where

S_g = g-sensitivity of crystal oscillator (g^{-1}).

$a(t)$ = applied acceleration (g).

Sinusoidal vibration with applied acceleration

$$a(t) = a \cos 2\pi f_v t \tag{3}$$

frequency modulates the nominal oscillator output

$$f(t) = f_o + S_g f_o a \cos 2\pi f_v t \tag{4}$$

where

a = vibration amplitude (g).

f_v = vibration frequency (Hz).

In a GPS receiver, the reference-oscillator frequency is multiplied to L-band, where it is used as an injection frequency for the received GPS signal. This conversion process results in a multiplication of frequency deviation. At the carrier-tracking-loop input, the effective vibration-induced phase variation, $\Delta\phi(t)$, is given by

$$\Delta\phi(t) = 2\pi \int \Delta f(t)\, dt + C \tag{5}$$

Assuming zero initial phase input

$$\Delta\phi(t) = \frac{S_g f_L a}{f_v} \sin 2\pi f_v t \qquad (6)$$

where

f_L = L-band injection frequency (Hz).

To minimize mean-square tracking error resulting from input noise and dynamics, the carrier-tracking loop is assumed to have the characteristics of a third-order Wiener filter.(1)* Phase error, $\phi_e(s)$, is therefore related to input phase variations by

$$\frac{\phi_e(s)}{\Delta\phi(s)} = \frac{s^3}{s^3 + 2\omega_n s^2 + 2\omega_n^2 s + \omega_n^3} \qquad (7)$$

Evaluating the magnitude of the system function given by Eq. (7) at the vibration frequency ($s = j2\pi f_v$), yields the following relationship for peak tracking-loop phase error, ϕ_e

$$\phi_e = \left[\frac{\left(\frac{5.24 f_v}{B_L}\right)^6}{1 + \left(\frac{5.24 f_v}{B_L}\right)^6}\right]^{0.5} \frac{S_g f_L a}{f_v} \qquad (8)$$

where

$$B_L = \frac{\omega_n}{1.2}$$

= single-sided loop noise bandwidth (Hz).

Figure 1 shows the effect of noise bandwidth on phase error as a function of frequency for a peak vibration amplitude of 1.0 g, and a crystal-oscillator g-sensitivity of 1×10^{-9}/g. Curve I is a reference plot of $\Delta\phi$, the peak input phase, and Curves II through V are plots of ϕ_e, all as a function of f_v. The plots of ϕ_e versus f_v show the strong dependence of maximum phase

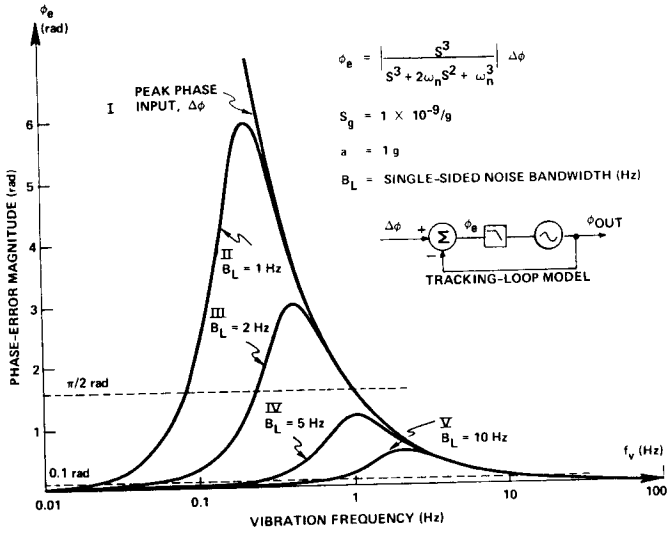

Figure 1. Effect of noise bandwidth on phase error (ϕ_e).

*Superscript numerals refer to similarly numbered references in the List of References.

error on loop noise bandwidth. At vibration frequencies below that at which each peak value occurs, phase error decreases as a direct consequence of the loop's ability to track the input variation. At frequencies above this value, phase error decreases because the input variation, following its $1/f_v$ dependence, is decreasing. The peak value occurs at the vibration angular frequency, ω_v, approximately equal to the loop's natural frequency, ω_n. More exactly, peak phase error occurs at

$$f_v = 0.214\, B_L \qquad (9)$$

Vibrations occurring between 0.1 and 1 Hz are sufficiently low in frequency to produce a large input phase variation, yet they are not low enough to be tracked by a narrow-bandwidth loop.

Combining the results given in Eq. (8) and (9) yields the following requirement for the g-sensitivity of a crystal oscillator for GPS receiver application

$$S_g \leq \frac{0.262\, B_L \phi_e}{f_L a} \quad (g^{-1}) \qquad (10)$$

where

ϕ_e = peak allowable phase error (rad).

Cases A and B of Figure 2 show this relationship for an allowable phase error of 0.628 and 0.1 rad, respectively. Both cases assume a peak acceleration of 1 g, and an L-band frequency

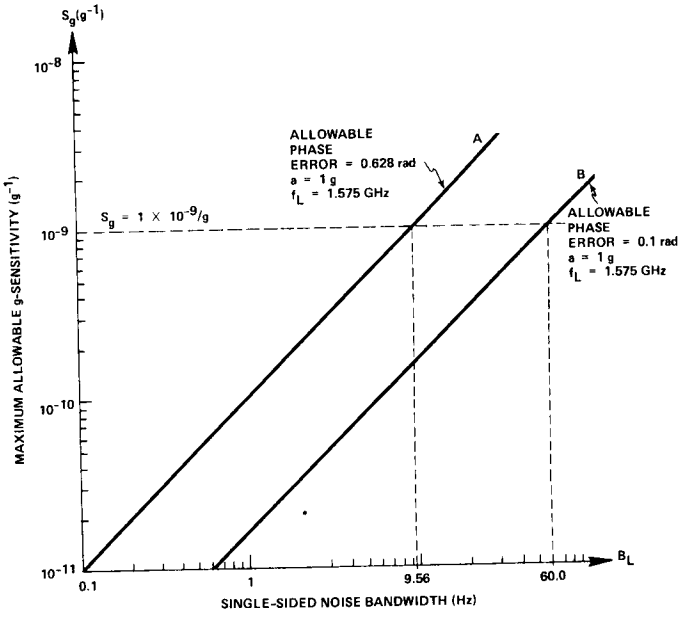

Figure 2. g-Sensitivity requirements as a function of noise bandwidth with 1-g vibration amplitude at worst-case vibration frequency.

of 1.575 GHz. GPS-qualified crystal oscillators with inherent g-sensitivities of about 1×10^{-9}/g impose lower limits of 9.56 Hz (Case A) and 60.0 Hz (Case B) on the minimum allowable one-sided noise bandwidth. Figure 2 graphically illustrates that vibratory forces with a 1.0-g peak value can limit A/J performance of GPS receivers by establishing lower bounds on tracking-loop bandwidths.

NONVIBRATORY-INDUCED PHASE ERRORS

In addition to the steady-state phase error produced by vibrations, peak phase errors occur during the transient response of the tracking loop to the changing dynamic environment produced by tactical aircraft maneuvers. As mentioned previously, such dynamics may be modeled as an applied step in jerk of 10.0 g/s, over an interval of 0.6 s.(2) Mechanical isolators have been shown to provide negligible attenuation of this input;(3) consequently, the acceleration applied to the oscillator is given by

$$a(t) = \int J(t)dt + C_1 \qquad (11)$$

where

$J(t)$ = step of jerk, $Ju_{-1}(t)$ (g/s).

With no initial acceleration assumed, the frequency deviation becomes

$$\Delta f(t) = S_g f_L J t \qquad (12)$$

Equation (5) is used to determine the effective phase input to the carrier-tracking loop.

$$\Delta\phi(t) = \pi S_g f_L J t^2 \qquad (13)$$

This input to the system described by Eq. (7) generates a response with a peak-phase overshoot that is approximately equal to the resulting steady-state phase error of a second-order loop with a frequency-rate step ($2\pi S_g f_L J$) applied.(4) The peak value of this error is

$$\phi_e \approx \frac{1.76 S_g f_L J}{B_L^2} \qquad B_L > 1.67 \text{ Hz} \qquad (14)$$

The requirement of crystal-oscillator g-sensitivity for GPS application becomes

$$S_g \leqslant \frac{0.568\ \phi_e B_L^2}{f_L J} \ (g^{-1}) \qquad B_L > 1.67 \text{ Hz} \qquad (15)$$

This relationship is presented in Figure 3 for allowable phase-error limits of 0.1 and 0.628 rad, using the previously described dynamic input. The corresponding minimum bandwidths are 6.64 and 16.6 Hz, respectively, with the assumed g-sensitivity of 1×10^{-9}/g. These results are based on a linear description of tracking-loop behavior, and therefore tend to be optimistic. Again, the crystal oscillator is seen to present a limiting factor to receiver capability. By affecting crystal-oscillator stability, aircraft dynamics, as well as vibrations, require wider bandwidths to preserve phase-error margins. Consequently, the A/J performance of the GPS receiver is significantly degraded.

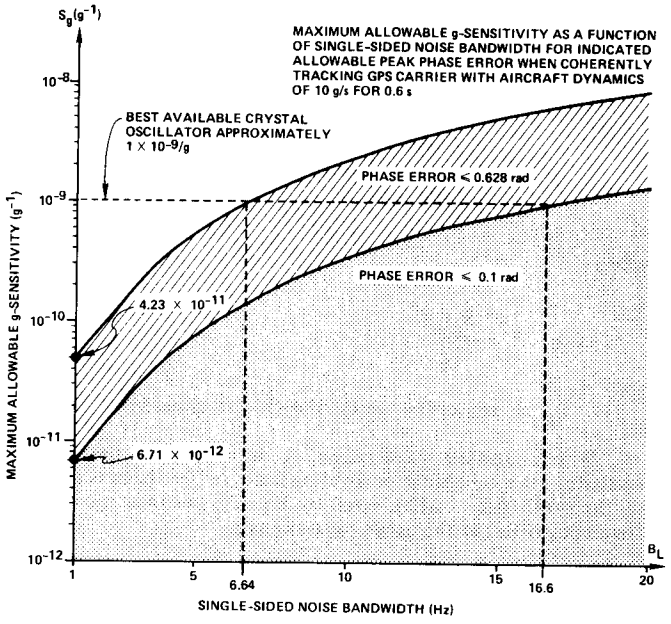

Figure 3. g-Sensitivity requirements of crystal oscillators for GPS applications.

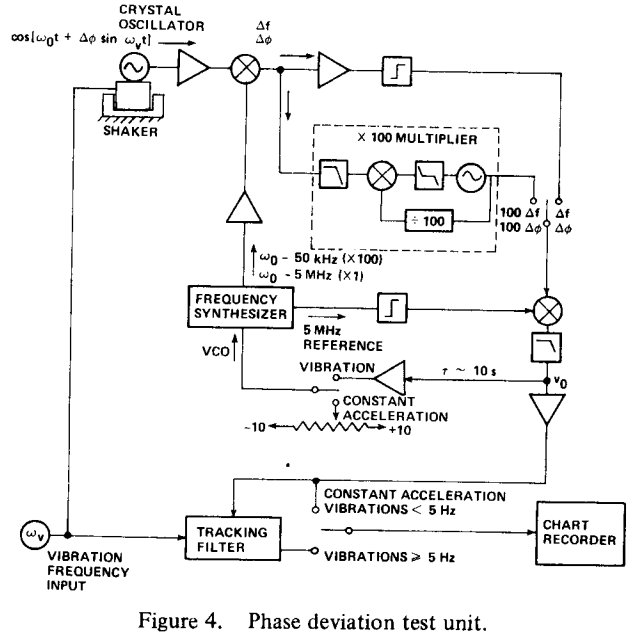

Figure 4. Phase deviation test unit.

DETERMINATION OF g-SENSITIVITY

Characterization of the crystal-oscillator g-sensitivity can be accomplished by measurement of oscillator frequency or phase deviation in the presence of constant acceleration or vibration, respectively. By testing the unit over a range of vibration amplitudes and frequencies, the g-sensitivity dependence on these parameters along any crystallographic axis may be determined. The system illustrated in Figure 4 has been designed to perform this task. Vibrations ranging in frequency from 1 to 100 Hz, with amplitudes (subject to shaker limitations) of up to 5 g, are applied to a crystal oscillator. Its center frequency, containing acceleration-induced phase variations, is down converted by mixing with a locally generated synthesized injection frequency. When amplification of the phase variation is required, a phase-locked loop will provide X100 multiplication at 5 MHz over the entire range of vibration frequencies. The resultant phase variation is then heterodyned to baseband by a local 5-MHz crystal oscillator, which also provides a reference for the synthesizer. During vibration tests, a portion of the filtered baseband signal is fed back to the synthesizer voltage-controlled frequency input to ensure a quadrature relationship at the baseband mixer, as well as

to remove long-term frequency changes without affecting vibration-induced phase deviations. The filtered baseband signal is assumed sinusoidal in nature. Its amplitude is proportional to the oscillator g-sensitivity.

$$v_o = \begin{bmatrix} \Delta\phi \\ \text{or} \\ 100\ \Delta\phi \end{bmatrix} \sin \omega_v t \qquad (16)$$

where

$$\Delta\phi = \frac{S_g f_o a}{f_v}$$

f_o = center frequency of oscillator under test.

When constant acceleration, A, is applied to the crystal oscillator via a centrifuge or dividing head, no feedback is applied to the synthesizer. $\Delta f(t)$, given by Eq. (2), becomes a constant frequency offset at the oscillator terminals.

$$\Delta f = S_g f_o A \qquad (17)$$

To maintain lock of the phase-multiplier loop, its output must be offset by 100 Δf. The filtered baseband signal now becomes

$$v_o = \sin 2\pi \begin{bmatrix} \Delta f \\ \text{or} \\ 100\ \Delta f \end{bmatrix} t \qquad (18)$$

In this mode it is the output frequency that is a measure of g-sensitivity. For both vibration and constant acceleration, information is processed using a tracking filter and chart recorder. A more convenient form of data acquisition is contemplated once availability of test data indicates the general character of the measured parameter.

Figure 5 shows a relationship between the test-unit measuring capability and the power levels in the vibration-induced sidebands that would adversely affect a GPS error budget of 0.1 rad at L band. All levels are referred to the oscillator terminals and are compared with the level of noise processes found in a typical GPS-qualified crystal oscillator.

SUMMARY

An analysis has indicated the inadequate performance of a crystal reference oscillator in a dynamic environment. Because mechanical isolation has little effect on slowly varying accelerations, some form of dynamic compensation is required to overcome the effects of g-sensitivity. This necessitates the determination of a suitable oscillator model. A g-sensitivity measurement system has been described which should enable such characterization.

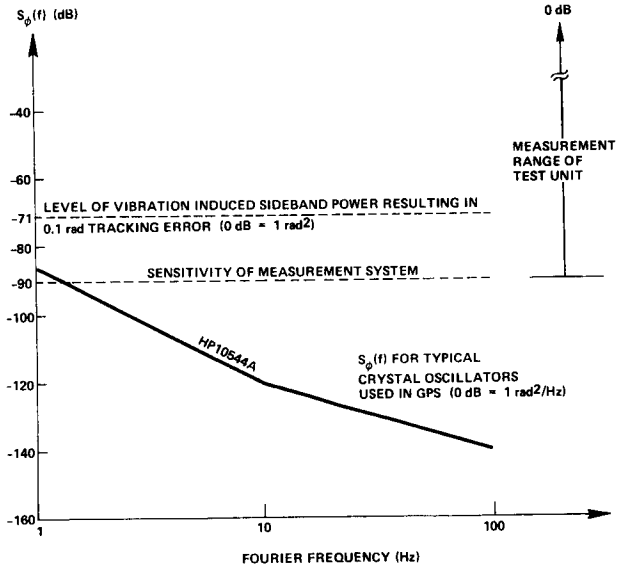

Figure 5. Comparison of modulation levels; vibration-induced sidebands measured at oscillation terminals vs. random-noise process.

ACKNOWLEDGMENT

The work reported in this paper was sponsored by the Air Force Avionics Laboratory (AFAL) under Project Number 6095 through USAF Contract F33615-75-C-1149. The project officers at AFAL were Capt. Edwin V. Harrington, Jr. (AFAL/RWA-2) and Neil Banke (AFAL/RWA-2).

Publication of this paper does not constitute approval by the U.S. Air Force of the findings or conclusions contained herein. It is published for the exchange and stimulation of ideas.

LIST OF REFERENCES

1. Jaffe, R., and E. Rechtin, "Design and Performance of Phase-Lock Loops Capable of Near-Optimum Performance over a Wide Range of Input Signals and Noise Levels", Trans, IRE, IT-1, March 1955, pp. 66-76.

2. C. R. Cahn et al., System 621B Signal Definition Study, SAMSO-TR-72-248, October 1972.

3. "GDM Performance with Carrier Tracking Bandwidth Limitations due to Crystal Oscillation G-Sensitivity", Internal Charles Stark Draper Laboratory Memo from P. Konop to Duncan Cox, 21 June 1976.

4. C. R. Cahn, Threshold Reduction of GPS Receiver by IMU Aiding, Magnavox Report MX-TM-3175-75, 30 May 1975.

A NAVSTAR/GPS SIMULATOR

Donald W. Candy

Texas Instruments Incorporated

ABSTRACT

A brief introduction to the Global Positioning System is given. The problem of real-time GPS simulation is studied. Design considerations for the implementation of a simulator system with desirable capabilities are explored. The general approach for the Texas Instruments GPS simulator is presented. Finally, the specific capabilities of the Texas Instruments simulator are discussed with respect to the real system.

INTRODUCTION

The NAVSTAR Global Positioning System (GPS) is a precision satellite navigation system being developed by the Air Force Space and Missile Systems Organization. GPS is a long-range development program scheduled to become fully operational in the mid-1980's. The program is in Phase I (concept validation) of a three-phase development sequence. Initial testing will begin this year at the Army's Yuma Proving Ground, near Yuma, Arizona. The first tests will use an inverted range in which ground transmitters are used instead of satellites. Within a year, six NAVSTAR satellites will be placed into orbit, providing approximately 4 hours test time per day at the Yuma site.

To provide system-level testing of a GPS navigation set before actual field testing requires a test system capable of modeling the relative motion between the navigation set and four or more NAVSTAR satellites and of producing GPS RF signals whose content and characteristics precisely simulate those received by user equipment in the real system. This paper describes such a system.

THE GLOBAL POSITIONING SYSTEM

The NAVSTAR/GPS system will consist of three major segments. These are as follows.

Space Segment

The space segment will provide 24 navigation satellites in earth orbit arranged to provide continuous world-wide coverage to users of the system. Each navigation satellite will transmit the signal structure shown in Table 1. The C/A and P-codes of each satellite are mutually exclusive and time-synchronous with the codes of all other satellites. Before carrier modulation, each code stream is biphase modulated with a data stream. The data stream contains information about the satellite necessary for the user to obtain a navigation solution. This information consists of:

- Clock bias and drift rate coefficients
- Ephemeris coefficients that precisely define the satellite's position as a function of time
- Information on satellite status and data integrity
- An almanac that provides ephemeris and clock information on all satellites in the system.

TABLE 1. SATELLITE DOWNLINK SIGNAL STRUCTURE

Carrier Frequencies:

L_1 – 1575.4 MHz (154 × 10.23)
L_2 – 1227.6 MHz (120 × 10.23)

P-code:

10.23 MHz pseudorandom code
Unique to each satellite
7 days long before repeating

C/A Code:

1.023 MHz pseudorandom code
Unique to each satellite
1 millisecond long before repeating
In quadrature with P-code

Data:

50 Hz nonreturn to zero
1500 bits before repeating
Double error detecting parity
Updated every hour from control segment

Carrier, P-code, C/A code, and data bit sync all coherent.

The C/A (clear/acquisition) code repeats every millisecond and is therefore easy to acquire. When acquired, the C/A code allows data to be read that contains handover information for P-code acquisition. The P-code repeats itself every 7 days. Each P-code state, therefore, represents time from the beginning of the week. A second L-band link (L_2) is provided to allow differential time-of-arrival measurement, permitting correction of L_1 propagation delay for ionospheric refraction. The L_2 link transmits either the P-code or the C/A code, but not both.

Ground Segment

The ground segment consists of several tracking stations, data processing systems, and an uplink to the space segment. The ground segment is responsible for computing precise ephemeris and time-correction data and uploading these data to the space segment.

User Segment

The function of the GPS user equipment is to:

- Select the "best" set of navigation satellites
- Acquire the satellite signals
- Read the satellite-transmitted data
- Measure range and range rate
- Calculate satellite position
- Calculate user's three-dimensional position, velocity, and time
- Perform coordinate transformation to aid operator use
- Display output for operator use.

Data from at least four satellites must be included in the navigation solution to solve for position, velocity, and user-clock time bias. The data can be obtained either simultaneously or sequentially. Obviously, the simultaneous measurements best suit high dynamic users such as fighter aircraft or missiles and the sequential measurements are sufficient for low dynamic users. Relative time-of-arrival measurements are made on specific code states or data transitions and the navigation solution is effected by solving four equations in four unknowns. Figure 1 shows this process.

The solution requires that the user lock onto four satellites, receive data from each, measure the relative time of arrival of a specific event in each signal, correct the measured times of arrival for bias and drift according to received data, determine from received data the position of the satellite at the time of transmission of that event, and use this information to effect a solution of user position and system time.

GPS USER EQUIPMENT TEST REQUIREMENTS

Three basic types of test equipment are necessary to provide the external stimuli required for development of a GPS user equipment system:

Dual-Frequency Static Signal Generator

This type of test equipment is needed for the early development phase to allow conceptual verification of receiver hardware design. Minimum functional capability for this type includes the P-code on L_1 only. The signal levels should be variable within the expected limits of the real system.

Dual-Frequency Dynamic Signal Generator

This type of generator is needed to test the response of the user equipment receiver design to the dynamics of its intended environment. In addition to the requirements for the static generator, the dynamic generator should provide the ability to offset the L-band signals in frequency by a time-varying doppler component to simulate the worst case dynamic situation between the user and a satellite. A single-channel unit using good analog synthesis techniques and capable of providing several preprogrammed dynamic scenarios is adequate for this purpose.

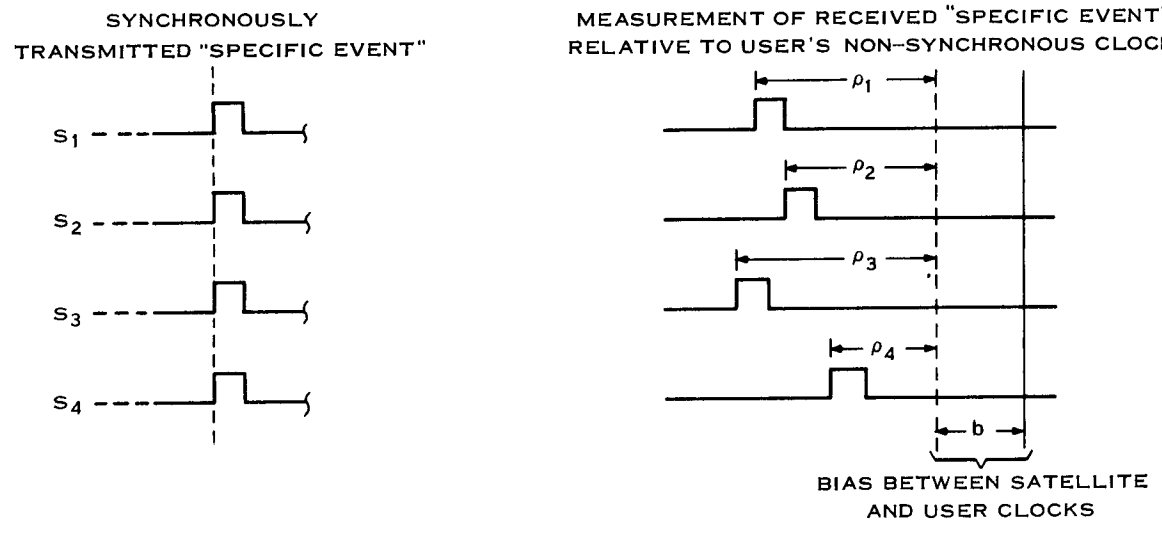

$$(R_i - B)^2 = (X_i - u)^2 + (Y_i - v)^2 + (Z_i - w)^2$$

WHERE: $B = bC$ AND $C = 3 \times 10^8$ m/s

$R_i = \rho_i C$

X_i, Y_i, Z = i^{th} SATELLITE POSITION AT TIME OF TRANSMISSION

u, v, w = USER POSITION

b = CLOCK BIAS BETWEEN USER AND SPACE SEGMENT

Figure 1. Illustration of Navigation Solution

Dual-Frequency Dynamic Simulator

This type of test equipment is needed to provide full system test capability for a GPS user equipment design. In addition to the capabilities provided by the static and dynamic generators, a GPS simulator of this type should provide as a minimum:

- Four or more channels to allow a navigation solution and full testing of the navigation section of a GPS user equipment.
- The ability to model and simulate the relative dynamics between a user trajectory and the orbits of four or more NAVSTAR satellites.
- The ability to model and control signal level and signal-to-noise ratio according to the geometric relationship of the user and the satellites.
- The ability to model and simulate intelligent jamming of NAVSTAR signals.
- The ability to model and simulate ionospheric delay of NAVSTAR signals.
- The ability to model and simulate reflected (multipath) NAVSTAR signals.
- The ability to model and simulate varying geometric dilution of precision situations.

Several distinct important advantages can be realized from a simulator with these capabilities. User equipment design can be more thoroughly tested in the laboratory before actual field testing. This is extremely important in the case of space- or missile-borne user equipment. The simulator can be used to reconstruct problems encountered in the field testing of ground or airborne equipments. New concepts in user equipment design can be laboratory tested and verified without costly field testing.

The simulator described by this paper is being developed by Texas Instruments.

TEXAS INSTRUMENTS NAVSTAR/GPS SIMULATOR

Ideally, a GPS simulator, however sophisticated, should encompass the requirements for the single-channel static and dynamic signal generators previously described. Also, the overall architecture should support varying degrees of sophistication so that the final configuration can be easily tailored to meet the varying requirements of the many types of users. A modular design concept has been used in the Texas Instruments simulator to ensure its usefulness in configurations of a wide variance of sophistication. Care has been taken to ensure that each level of sophistication fully supports all lower levels. To facilitate the presentation of the simulator, it is described at its highest level of sophistication, followed by a description of its utility at lower levels.

A functional block diagram of the simulator is shown in Figure 2. The major subsystems are a modeling subsystem and a simulation subsystem.

In this configuration, the 990/10 computer doubles as the modeling subsystem data processor and the simulation subsystem data processor. The modeling subsystem receives inputs from the operator defining the situation to be modeled, models that situation, and outputs initialization parameters and real-time simulation drive parameters in the form of a simulation data base to one of the DS-50 disk units. The simulation subsystem operates under its own real-time operating system, which is bootstrap-loaded from the simulation data base disk. This system communicates with the operator through the 733 data terminal and uses the modeled drive parameters on the data base disk to drive the satellite simulators. This system architecture allows the subsystems to be separately located without impact to the basic subsystem structure or software.

Modeling Subsystem

The modeling subsystem hardware consists of a Texas Instruments 990/10 Software Development Facility including a 990/10 computer, two DS-50 disk drives, two 913A video display terminals, a 733 ASR data terminal, a card reader, and a line printer. The modeling subsystem software operates under control of the Texas Instruments DX-10 operating system and is written in FORTRAN. The DX-10 software development system provides a wide variety of software development aids such as a FORTRAN compiler, a 990/10 macro-assembler, a link editor, and an on-line debug package. The 990/10 system was chosen because of its software compatibility with the Texas Instruments SBP 9900 microprocessor used in all Texas Instruments user equipment development programs. The use of a software compatible computer maximizes the use of GPS-oriented personnel, documentation procedures, and configuration control procedures. It also assures the user equipment customer of a "standardized software system" throughout the program.

The modeling subsystem functional flow diagram is shown in Figure 3. The scenario generator software module provides the man/machine interface for operator definition of the situation or scenario to be modeled. The primary interface is the 913A Video Display Terminal; however, certain data such as the user trajectory and orbital ephemerides are entered via the card reader. The scenario generator organizes these data into files and tables that are readily accessed by the modeling program.

The scenario modeler software cubic curve fits the course points of the operator-defined user trajectory and interpolates user position to the 1-millisecond periods. The orbital equations for each satellite are interpolated to the same resolution and the radial displacement between each satellite/user pair is computed. The satellite is offset in its orbital position with respect to time to allow for propagation delay of the L-band signals. To "close the loop," the modeler emulates the simulation subsystem hardware and considers its response in the generation of each drive constant.

The final product of the modeling subsystem is the simulation data base disk. This disk may contain many scenarios to provide a variety of test situations to the user equipment. The ultimate real-time capacity of the disk is approximately 2 hours.

Simulation Subsystem

The block diagram of the simulation subsystem is shown in Figure 4. The area outlined in dashes is a single channel and is identical for each of the eight channels. The data processor

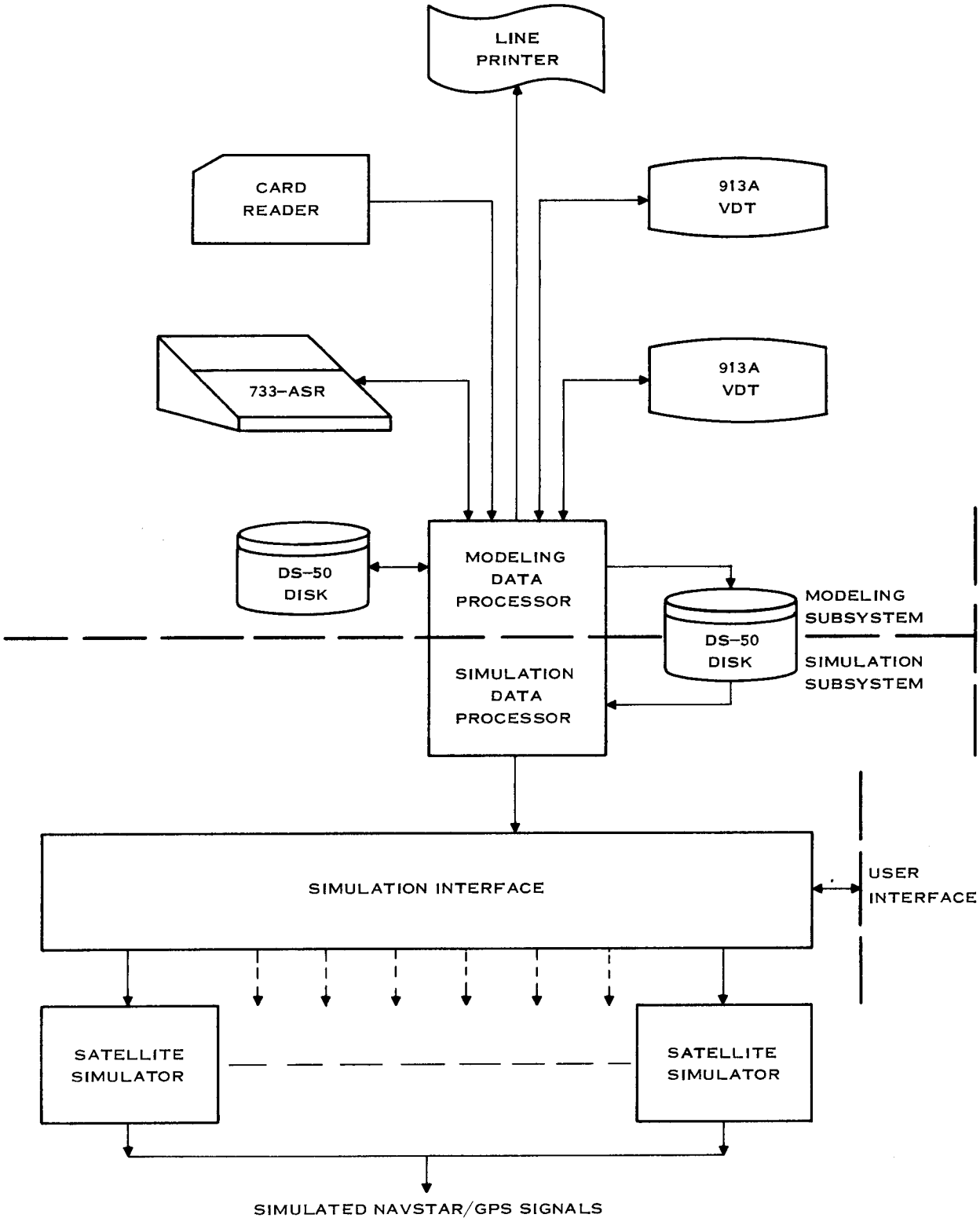

Figure 2. GPS Simulator Functional Block Diagram

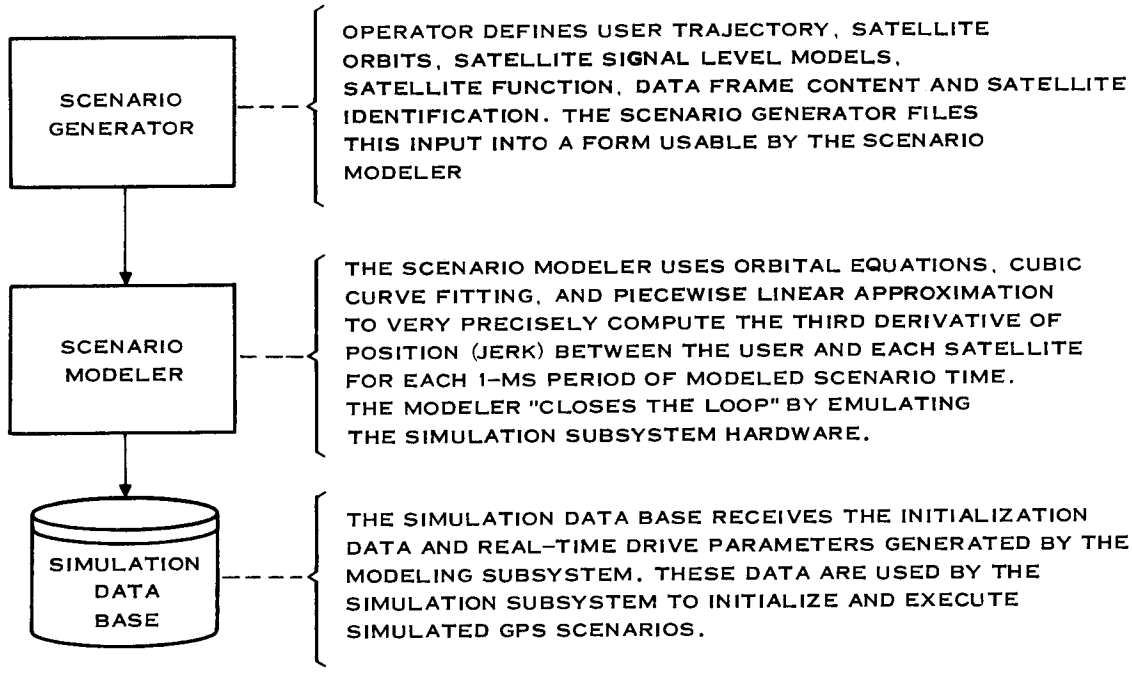

Figure 3. Modeling Subsystem Functional Flow

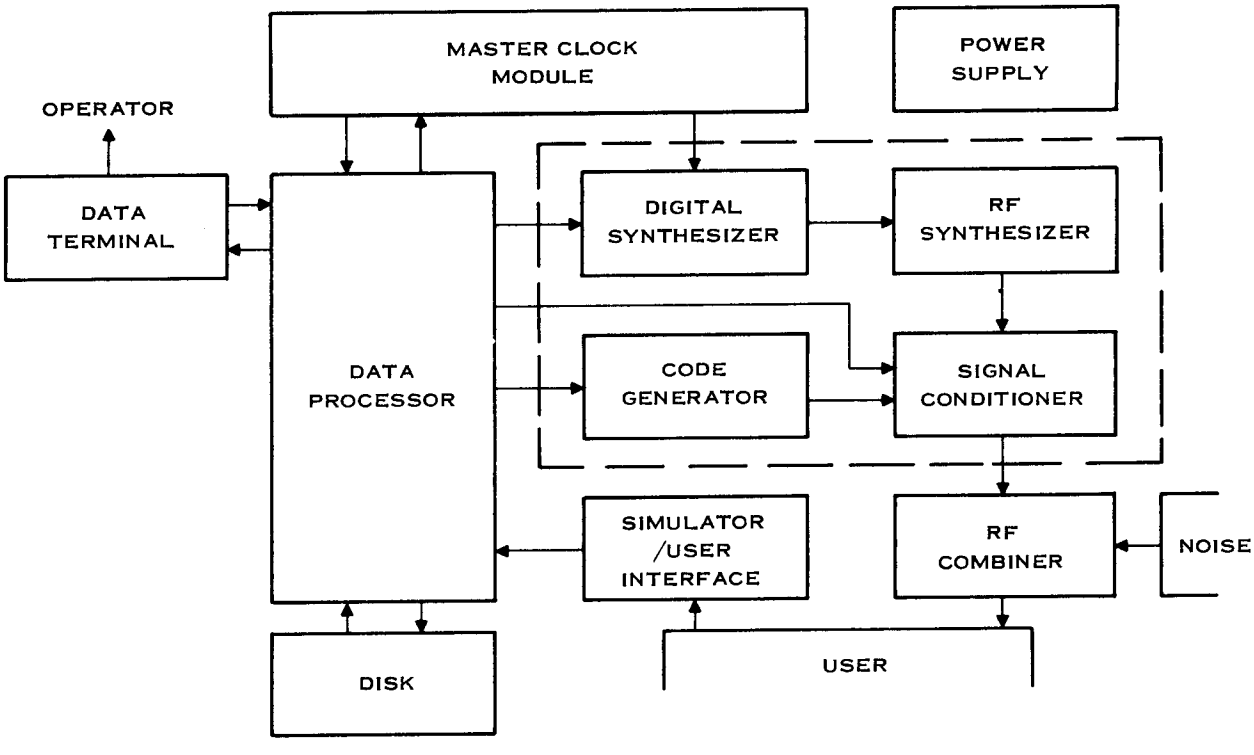

Figure 4. Simulation Subsystem Block Diagram

receives all real-time inputs from the simulation data base disk. The processor uses these inputs to drive the digital synthesizer, code generator, and signal conditioner modules of each channel.

The digital synthesizer receives jerk* data from the processor every millisecond. These data are triple-integrated to phase (position) with a doppler (velocity) resolution of approximately 30 μHz at 10.23 MHz (f_0). The phase resolution at f_0 is approximately 190 microradians, equivalent to 1.7 degrees at L-band. In addition to its precise phase resolution, the digital synthesizer exhibits perfect long-term stability with respect to the source and very good short-term stability. The perfect long-term stability is the feature that allows "closing the loop" in the modeling software.

The RF synthesizer module up-converts f_0 to 120 f_0 (L_2) and 154 f_0 (L_1) to provide the L-band simulated signal sources. It also provides a 17 f_0 reference for the code generation module.

The code generator module uses the doppler-corrupted 17 f_0 reference to generate the P- and C/A-codes. The P-code can be initialized and started at any time of the week. A vernier capability is provided to allow code state alignment to within 5.75 nanoseconds. The processor provides GPS data to the code generator for biphase (modulo-2) modulation of the code streams.

The signal conditioner module provides 42-dB dynamic attenuation of the L-band signals under processor control. It also provides the quadraphase modulation of L_1 and L_2 with the code streams and recombination of the quadrature components.

The master clock module contains a precise 10-MHz oscillator. This clock is the time reference for the entire simulation subsystem. All submultiples of 10 MHz, used for synthesis, processor interrupts, and timing, are generated in this module.

The RF combiner module combines the modulated L-band signals from all channels and provides a final stage of manually variable attenuation. An additional combination stage is provided for the injection of noise, if desired.

The simulator/user interface module is designed to allow the simulation data processor to extract data from the user during real-time operation. The processor stores these data on the simulation data base disk in an area provided for this purpose. This allows postsimulation analysis of user response to the simulation scenario.

The operator communicates with the simulation subsystem through the 733-KSR data terminal. Upon initialization of the subsystem (bootstrap process), the operator has a choice of four operational modes: full simulation, collinear motion simulation, calibration, and diagnostics. The full simulation mode requires the selection and initialization of one of the simulation scenarios provided on the simulation data base disk. The collinear motion mode allows the operator to initialize a single simulator channel to present a constant velocity, acceleration, or jerk to the user. The operator can also specify and generate a continuous combination of constant velocity, acceleration, and jerk segments in this mode. Signal levels can be specified as a function of time in the collinear motion mode.

The calibration mode is provided to allow software calibration of the processor-controlled attenuators and of interchannel TTL delays. The calibration parameter tables are maintained on the data base disk and "booted" in during subsystem initialization. The diagnostic mode is provided as a field troubleshooting aid. Diagnostic software includes disk, processor, simulator channel, and user. The user diagnostics are downloaded through a user maintenance port (not shown). The user diagnostic software gives the simulation subsystem 990/10 processor "maintenance control" over the SBP 9900 microprocessors in the Texas Instruments user equipment. This is another important advantage in the software compatibility of the Texas Instruments 990 family in this application.

SIMULATOR UTILITY

The Texas Instruments NAVSTAR/GPS simulator can be configured to meet the requirements of a wide variety of user applications. The overall system architecture and design supports all configurations. The subsystem software is identical for all configurations. The hardware design uses the modular "plug-in" concept. The simplest configuration of the simulation subsystem consists of:

- 1 733-ASR data terminal (with cassette loader)
- 1 990/10 computer with 16K memory
- 1 Power supply drawer
- 1 Master clock module
- 1 Simulator channel
- 1 RF combiner assembly.

This configuration will allow collinear motion simulation on one channel. The addition of one DS-50 disk unit will add the capability of full simulation on one channel. This configuration can operate sequentially to allow a navigation solution in a single-receiver user equipment. The addition of three simulator channels will allow a navigation solution in a multireceiver user. Up to four auxiliary channels can be added to greatly increase the capability of user testing. An eight-channel system will allow the following types of testing.

Fully modeled ionospheric. This test requires two simulator channels per satellite. L_1 is generated by one channel and L_2 by the other. The varying ionospheric delay is modeled into the L_1/L_2 pair.

Multipath testing. Multipath rejection can be tested by using a modeled "ghost" channel, delayed slightly from the primary channel.

Constellation testing. When a user equipment is presented with more than four satellites, it must pick the four that provide the least amount of geometric dilution of precision and, hence, the best navigation solution. Complex but realistic situations can be modeled to test the user response to boundary conditions between two or more constellations.

Intelligent jamming. One or more auxiliary channels can be initialized as a jamming satellite in order to test the user equipment's rejection of unwanted signals.

*Jerk is the time rate of change of acceleration.

This system can be expanded to a modeling/simulation system by adding one DS-50 disk unit, one 913A video display unit, one card reader, and one line printer.

CONCLUSIONS

The NAVSTAR/GPS simulator described by this paper will provide the necessary external stimuli to allow complex system-level testing of all types of GPS user equipment. Table 2 is a summary of the capabilities of this simulator.

TABLE 2. NAVSTAR/GPS SIMULATOR CAPABILITIES

Modeling Input

- User trajectory data
- Satellite ephemerides
- Satellite data frame content
- Signal-level modeling coefficients
- Simulator channel functional assignments

Simulation Output

- Simultaneous L_1 and L_2 RF signals
- P-code and C/A code on L_1
- P-code or C/A code on L_2
- GPS data on P- and C/A-codes
- Doppler corruption of all signals
- Dynamic signal level control

Simulator Characteristics

- Less than 1-meter error CEP
- 4.6 millihertz synthesis resolution at L_1
- Less than 2 degree phase jitter at L_1
- Expandable modular configuration
- User data recording capability
- Software-aided calibration
- Processor-controlled diagnostics